INVESTIGATION OF DIFFERENT MYOCARDIAL INFARCTION MODELS WITH DIFFERENT IMAGING MODALITIES

PhD thesis

Edit Éva Lukács M.D.

Heart Institute
Faculty of Medicine
University of Pécs

Leader of Doctoral School:

Prof. Sámuel Komoly M.D., Ph.D., DSc.

Leader of program:

Prof. Erzsébet Rőth M.D., Ph.D., DSc.

Prof. Ákos Koller M.D., Ph.D., DSc.

Leader of project:

Iván Horváth M.D., Ph.D., FESC.

Pécs, 2013

List of abbreviations:

ANOVA - analysis of variance
AUC - area under the curve
BV - bipolar voltage
CI - confidence interval
cMRI - cardiovascular magnetic resonance imaging
Cx - circumflex artery
EDV - end-diastolic volume
EDWT - end-diastolic wall thickness
ESV - end-systolic volume
ESWT - end-systolic wall thickness
EMM - electromechanical mapping
FWHM - full-width-half-maximum
Gd(DTPA-BMA) - gadodiamide
LAD - left anterior descending artery
LLS - linear local shortening
LVmassED - left ventricular mass at the end diastole
MI - myocardial infarction
ROC - receiver operator characteristics
SEM - standard error of mean
SI - signal intensity
SV - stroke volume
T% - infarct transmurality
UV - unipolar voltage
VF - ventricular fibrillation
WM - wall motion
WT - wall thickening

Table of contents

1. INTRODUCTION

1.1 Review of the literature

Myocardial infarction (MI) with the loss of myocardium and the consequent remodeling and heart failure is still the leading cause of mortality in the industrialized countries, despite the trend toward the decreasing 30-day mortality [1, 2]. Early successful reperfusion therapy results in myocardial salvage within the area at risk and decreases the prevalence of left ventricular remodeling and congestive heart failure [2]. The degree of infarct expansion and the intensity of remodeling depend on the time of revascularization. This phenomenon was first described by Reimer et al. in 1977 in canine models where coronary occlusion was applied for different time frames, and resulted in an inverse relation between the time to reperfusion and the size and transmural extent of the infarct [3]. On the other hand reestablishment of blood flow is beneficial outside that time frame, which could result in myocardial salvage. This was designated as the time-independent effects of an opened infarct related artery by Kim and Braunwald [4]. The late restoration of coronary blood flow promotes infarct healing and could prevent the process of expansion, aneurysm formation or electrical instability. Percutaneous coronary interventions allow achieving reperfusion in acute coronary syndromes; however there are still a portion of patients who could not receive any reperfusion therapy within the desired time range. It is still of high prognostic importance to evaluate the size of the infarct related area and to determine myocardial viability among these patients in order to estimate the benefit of planned revascularization procedures.

1.2 Animal models - Importance of interspecies differences and the methods for the induction of MI

From the numerous animal models of regional myocardial ischemia, the in vivo models are preferred in large animals, since the ethical, practical and financial issues associated with the study of human tissue. There are several aspects that need to be taken into account at the early designing phase of experiments, since they could have significant influence, resulting in misleading interpretations. First of all one should pay attention on the interspecies difference of the two most utilized animals in

the field of cardiovascular research: dogs and porcine. The dog heart consists of large epicardial interarterial collaterals, and the distribution of the vasculature mainly shows left dominance [5, 6], which is most infrequently seen in humans. The heart of porcine species closely resembles to the human heart, regarding the distribution of coronary arteries [7] and the small amount of collaterals [5, 8]. Hearse et al. and Verdouw et al. suggested that porcine hearts characterized by small amount of collaterals resemble to the early phase of human disease, and dogs with extensive collaterals resemble the features of patients with chronic coronary artery disease [9, 10]. Other important aspect of experimental design is the difference in the surgical methods of MI induction e.g. the application of open or closed chest methods. Open chest models are usually characterized by increased mortality and complication rates [11]. Open chest methods induce increased surgical trauma and inflammation moreover infections could occur more often [12]. The scar tissue formation and the increased presence of air in the tissue layers also influence the local anatomical settings, which could deteriorate cMRI image quality [13]. Pericardial incision also could affect intrathoracic pressures and hemodynamics [14], while hypothermia [15] and body temperature in the normothermic range [16] significantly affects infarct size. The catheter-based minimal invasive interventional cardiology techniques allowed the wide application of the closed chest methods for the in vivo evaluation of MI and are preferable regarding the better survival rates, time and cost consumption [11]. Furthermore the closed chest methods allow longer follow-up time after therapeutic interventions, promoting further the better and more critical interpretation. Large animal models, e.g. porcine, dog, sheep or baboons enable the utilization of catheter-based techniques in contrast to small animals. Consequently, as mentioned above large animals, especially the porcine heart highly resembles the features of humans. Finally as it was summarized by Hearse and colleagues, large animal models are the most relevant concerning physiology and the daily clinical routine, they allow to perform follow-up studies, in an intact animal in vivo, and they enable the use of all the techniques and measurements, which are used in the clinical practice, such as percutaneous coronary intervention techniques, echocardiography and magnetic resonance imaging. The disadvantage of large animal models could be the fact that the experimental process of MI induction takes place in healthy animals, which differs mainly from the complex and progressive development of human disease, influenced by many genetical and environmental factors. These differences

could play important role in the contrasting results regarding the effects of infarct size limiting drugs, since these interventions produced significant infarct size limiting effects in animal models, but failed in man [9].

1.3 Reperfused and nonreperfused MI - Patophysiological background

As it was emphasized in the review article of Pfeffer and Braunwald the prevalence of left ventricular remodeling and the consequent heart failure, adverse events and increased mortality can be best influenced by the limitation of the "initial insult" [2]. It was already demonstrated from the early animal experiments of MI, that restoration of blood flow facilitates myocardial salvage [3, 17]. According to the results of Garcia-Dorado et al., longer than 30 minutes occlusions result in exponential increase of infarct size, and could reach up to 75% of the infarct area of animals with permanent occlusion at 90 minutes [17]. In other words, in the absence of significant collaterals 120 minutes of occlusion results in a complete infarction, while the necrosis can be prevented within 30 minutes of occlusion. On the other hand the difference of collateral circulation among species should also take into account, since pigs are characterized by poor collaterals in contrast to the dog, which have well developed collaterals. In dogs nearly 50% of the myocardium at risk could be salvaged with reperfusion after 90 minutes [18]. In 1971 Maroko et al. described other factors that can influence infarct size beside the time from occlusion to reperfusion using open-chest dog MI models via the examination of the extent and magnitude of epicardial ST segment elevation. Certain factors can influence the balance between oxygen supply and demand. For instance the induction of tachycardia via the administration of isoproterenol results in a more intensive myocardial injury, in contrast to the administration of propranolol [19]. Myocardial reperfusion could result in reversible and irreversible injuries, due to oxygen derived free radicals and calcium overload. In the injured myocardial tissue platelet deposition is accompanied by the migration of neutrophils. This process is associated with coronary endothelial dysfunction, and the rapid entry of neutrophils occurs especially after reperfusion. According to Kloner four types of reperfusion injury could be observed in experimental animals: lethal reperfusion injury, referring reperfusion induced death of still viable cells, vascular reperfusion injury, which manifests as microvascular damage, stunned myocardium, which is demonstrated

through the contractile dysfunction of salvaged myocytes, and reperfusion arrhythmias, such as ventricular tachycardia or fibrillation [20]. Early reperfusion allows myocardial salvage, prevents the process of remodeling, left ventricular dilatation, heart failure and electrical instability [4], despite the above mentioned factors of reperfusion injury. In the cases of chronic occlusions, where no reperfusion occurs, the process of myocardial remodeling results in decreased survival through the increased prevalence of heart failure and malignant ventricular arrhythmias [2]. Since the difference in the prevalence of left ventricular remodeling, heart failure and mortality, myocardial infarcts with or without reperfusion represents different patophysiological and clinical entities. According to this fact the preclinical studies also should aim to point out this difference in animal models for the evaluation for both diagnostic methods and therapeutic approaches.

2. Aims

There are five different types of acute MI, as it is already known even from the everyday clinical practice and guidelines [21]. Although several diagnostic approaches are available to aid more effective and oriented therapy, the patophysiological background, e.g. the presence or absence of reperfusion significantly influences this pursuit. The reperfused and nonreperfused MI have different outcomes [4] and could require the involvement of new biological therapeutic approaches, therefore feasible methods are required to provide information about myocardial viability for every clinical settings. Our main aim was to apply different reperfused and nonreperfused porcine models of MI and to evaluate them via electromechanical mapping (EMM), as an invasive diagnostic method for the detection of myocardial viability, regarding the different pathomechanism and location with the additional utilization of cMRI as a gold standard non-invasive method. Although the value of EMM has been already evaluated by several animal and clinical studies, they lack the systematic investigation of EMM in reperfused and nonreperfused MI models, using the same protocol. Partially, we investigated (1) the applicability of the different reperfused and nonreperfused MI models, (2) the relationship between the parameters of global left ventricular function and the UV, BV and LLS values, (3) the differences in the grouped UV, BV values according to the cMRI viability and transmurality results using the same regional segmentation. Finally, since EMM has limited diagnostic accuracy in the posterobasal region [22], we also induced MI in the territory of the Cx artery using coil embolization, in order to perform ROC analysis according to the different anatomical localizations (LAD or Cx).

3. Investigation of porcine MI models, implication of different occlusion methods

3.1 Reperfused and nonreperfused MI - Experimental settings

The different methods for the induction of myocardial necrosis result from different patomechanical processes in preclinical models while the reperfused and nonreperfused MI also have different outcomes [4]. The transient occlusion methods most frequently serve a platform to evaluate the effects of pharmacological agents in the prevention of infarct expansion and reperfusion injury. The time frame of 90 minutes balloon occlusion allows still a small portion of the myocardium to be salvaged [3], this method is used most frequently in closed-chest large animal models [23-27], and were earlier induced by ligation techniques in open-chest models [3, 17, 19].

The open chest methods allow both the utilization of permanent or temporary occlusions, via ligation [3, 28], vascular clamps [19], snare [29], hydraulic [30] and pneumatic occluders [31]. The direct visual control of hyperaemia at reperfusion and the measurement of contractile function [32], metabolic parameters [33] or gross morphologic details of cardiac ischemia in vivo [34] are the main advantages of these methods, although they are usually characterized by increased mortality and complication rates [11]. Inflammation and infections could occur more often [12], and they could induce increased surgical trauma. During the postoperative stage the scar tissue formation and the increased presence of air in the tissue layers could deteriorate cMRI image quality [13]. Hypothermia is widely used in open-chest methods, although it significantly could affect the infarct size [15]. Large animal models serve as candidates for the testing of novel minimally invasive heart surgery techniques, such as endoscopic approach of the internal mammary artery [35].

The catheter-based minimal invasive interventional cardiology techniques allowed the wide application of the closed chest methods for the in vivo evaluation of MI and are preferable regarding the better survival rates, time and cost consumption [11]. Temporary occlusions can be achieved by the utilization of balloon inflation [23-27, 36] or application of balls with an attached filament [37] in the coronary artery. Permanent occlusion could be induced via embolization materials, e.g. graded microspheres [38], coils [39-41], foam sponge [42], agarose

gel beads [43], or application of endothelial electrical injury [44], heating of a thermosonde [45]. The main characteristics of these models are summarized in Appendix 1.

3.2 Aims

Despite the above mentioned large amount of data, the parallel evaluations of the different closed chest MI models are lacking. Therefore in the first part we investigated the differences in mortality and complication rates in the balloon occlusion and coil deployment methods.

3.3 Study design

MI was induced using either balloon occlusion (n=7) of the left anterior descending artery (LAD) for 90 minutes followed by reperfusion, or percutaneous embolization coil deployment (n=9) in the LAD (n=6) or the circumflex artery (Cx, n=3). The cMRI and EMM procedure were performed at the sixth day after the infarction induction procedure.

3.4 Porcine MI models

Anaesthesia was induced using intramuscular ketamine 15 mg/kg (10% Ketavet 100, Intervet International GmbH.) and xylazine 0.1 mg/kg (2% Primazin, Alfasan International B.V.) in sixteen domestic pigs weighing approximately 26 to 38 kg. After the induction of anaesthesia the animals were intubated and ventilated, using Isoflurane 2% and Oxygen 2-3L/min. Vital signs and electrocardiogram were monitored continuously. Each animal received 150 mg amiodarone (Cordarone) before the procedure in order to avoid malignant ventricular arrhythmias. The main steps of the preparation of the animals are presented on Figure 1. Five French sheath and Amplatz 1 or 2 guiding catheters were used to perform coronary angiography of the left coronary system after the preparation of the right femoral artery. Unfractionated heparine (90 IU/kg) were administered intraarterially before the angiography. In the balloon occlusion group (Cross sail, Guidant, Santa Clara, CA) anterior infarction was produced by transient (90 min) occlusion in the LAD after the

origin of the first diagonal branch, followed by reperfusion. Complete coronary occlusion was confirmed by angiography (TIMI flow score=0), beside the ST segment changes observed on the ECG. The reperfusion in the balloon occlusion group was also detected via angiography. In the nonreperfused MI group the coil (VortX, Boston Scientific, Natick, MA, USA) was deployed either in the LAD after the first diagonal branch or in the proximal part of the Cx artery according to the coronary angiogram. The occlusion was confirmed by angiography (TIMI flow score=0). Each animal received 100 mg magnesium and 1000 IU unfractionated heparine every thirty minutes during the balloon occlusion procedure. After the embolization procedure occlusion occurred within minutes. In the first hour of recovery prophylactic antibiotics (Shotapen, Virbac S.A.) were given intramuscularly and all animals were monitored for vital signs and signs of uncomfort. During the first week all animals in the LAD balloon group received Aspirin 100 mg daily. All animal experiments were carried out according to the regulations of the local institutional ethical committee and the Guide for the Care and Use of Laboratory Animals.

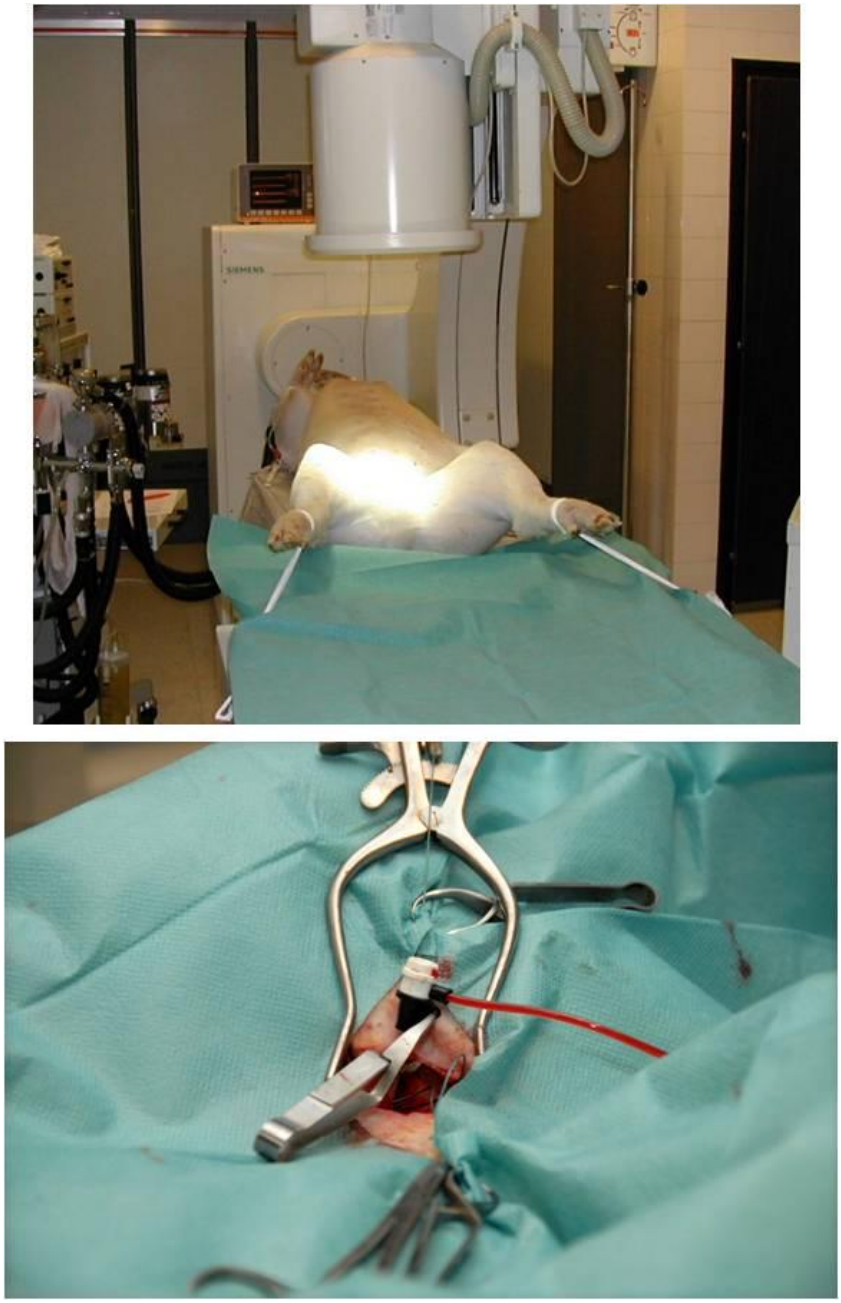

Figure 1. Illustration of the preparation of animals before the induction of MI. The upper part represents the positioning of the animal before the angiography; the bottom picture represents the inserted sheat in the right femoral artery.

3.5 Results

3.5.1 Mortality rates

The EMM and cMRI information of five animals in the LAD balloon group and 3-3 animals in the LAD and Cx coil groups were available at the sixth day for statistical analysis. Three animals from the LAD coil group (mortality rate: 50%) and 2 animals from the LAD balloon group (mortality rate: 28.57%) died during the procedure, at the time of occlusion or right after balloon deflation due to fatal ventricular fibrillation. All animal survived in the Cx coil group, although one animal showed signs of pulmonary oedema on the fifth day post MI. The overall mortality rate was 31.25%.

3.5.2 Occurrence of malignant arrhythmias

Despite all animals received amiodarone as a premedication the occurrence of ventricular arrhythmias were frequent, and were treated by 150J DC shock and additional intravenous magnesium. The rates of non-fatal ventricular arrhythmias were the following: 28.57% in the LAD balloon group, 33.33% in the LAD coil group. Arrhythmia was not observed in the Cx coil group.

3.5.3 Occurrence of other perioperative complications

In the LAD coil group one animal suffered from abdominal haemorrhage according to the post-mortem autopsy, which we referred as a surgical complication and vascular rupture after the preparation of the femoral artery. During the coil deployment procedure we observed extravasation on coronary angiography, which ceased after additional coil deployment in one animal in the Cx coil group.

3.6 Discussion

The balloon occlusion model represents the features of reperfused MI [23, 25] and furthermore demonstrates the changes which are consistent with the clinical data in the cases of primary percutaneous coronary intervention in acute coronary syndromes. Embolization materials, e.g. coils are used to induce permanent occlusion of the coronary artery and these methods resemble the features of nonreperfused MI [40]. The sign of no-reflow phenomenon on the cMRI images represents the phenomenon of microvascular obstruction, which predicts increased left ventricular remodeling [46] and correlates with a higher rate of cardiovascular events in the first two years after MI [47]. It is detectable in the cases of reperfused myocardial infarcts and was present in our experiments also, in the LAD balloon group. As mentioned before no reperfusion occurs in the permanent occlusion models, and the wavefront phenomenon of myocardial necrosis is complete [3], serving as a good approach for the clinical situation where we are not able to achieve revascularization, e.g. in no-option patients. The coil deployment method [13, 39-41, 48], allows precise positioning of the occlusion in the coronary artery, to produce similar area at risk, and moreover produces no artefacts on cMRI images, due to its MRI compatible material. This model closely resembles to the human course of atherosclerotic disease superimposed by thrombus formation [39]. Both models provide appropriate platform for the evaluation of novel regenerative therapeutic approaches such as growth factor and cell therapies. Recent metaanalysis of van der Spoel et al. demonstrated that permanent occlusion models are associated with more improvement, than the transient occlusion models after cell therapy [49], which could result from the larger infarct expansion, occurring without reperfusion and myocardial salvage in contrast to the temporary occlusion models. This result also emphasizes the involvement of both models in preclinical studies. The mortality rates in our MI groups did not differ significantly in cases of LAD occlusion using either balloon or coil deployment, producing similar area at risk. Death most frequently resulted from ventricular fibrillations, resistant against repeated DC shocks and antiarrhythmic therapy. Mortality rate could vary between 20 and 50% in different catheter based techniques [13, 26, 36, 40, 42, 43, 50] and were 33.33% and 28.57% in our practice in the coil deployment (nonreperfused) and balloon inflation (reperfused) induced groups, respectively. It is well known from the literature, that

the reversibility or irreversibility of myocardial injury and the size of myocardial infarction depend on the time course [3, 32] and localization of occlusion [28]. Usually the large diagonals are playing important landmark role on the LAD during the positioning of the occlusion. On the other hand Huang et al. raised a practical new approach in open chest models, since they used the whole length of LAD as a landmark, rather than its diagonal branches to produce similar area at risk [51]. In our experience both the 90 minutes balloon occlusion and the coil deployment in the LAD produced similar myocardial infarct size, using diagonal branches for landmarks in both model. The reproducibility of infarct size plays an important role, since in preclinical studies of stem cell therapy usually results in a left ventricular ejection fraction improvement of less than 10% [49]. The exact angiographic determination of similar occlusion sites ensures this demand.

4. Determination of global and regional left ventricular function in porcine MI models: invasive and non-invasive modalities

4.1 Introduction

Early successful reperfusion therapy results in myocardial salvage within the area at risk, therefore decreases infarct size, ventricular wall stress, dilatation and the prevalence of left ventricular remodeling and congestive heart failure [2]. The degree of infarct expansion determines the intensity of remodeling, together with the process of infarct healing and the consequent changes in ventricular wall stresses. Early revascularization attenuates this process. The survival after MI is influenced negatively by the left ventricular end-diastolic and end systolic volumes, and positively by the ejection fraction [52]. Cardiac MRI played important role in the evaluation of the cardiac performance from the mid-1980s [53], due to its high spatial and temporal resolution. Both the values of global and regional left ventricular function are measured in end-systole and end-diastole. The above mentioned high spatial and temporal resolution allows the exact quantification of regional wall thickness, systolic wall-thickening (absolute or percentual values). The preserved wall thickness is a good indicator of myocardial viability in chronic myocardial infarctions [54]. In patients with heart failure the measurement of ejection fraction and left ventricular volumes via echocardiography, contrast ventriculography, radionuclide ventriculography and cMRI are not interchangeable [55]. Echocardiography and contrast ventriculography usually overestimates the value of ejection fraction. Recent evaluation of the effects of stem cell therapy in large animal models indicated, that stem cell therapy improves left ventricular ejection fraction by 7,5% [56]. This fact highlights the importance of the exact evaluation of left ventricular function, before biological therapies and during the follow-up period.

In vivo mapping and navigation combined with an electrophysiological catheter to perform left ventricular electromechanical mapping (EMM) was first introduced by Ben-Haim et al in 1996 [57]. Since then EMM was widely investigated regarding the diagnostic accuracy of this method in both preclinical and clinical settings of ischemic cardiomyopathy [22, 58] and in experimental non-ischemic cardiomyopathy [59]. EMM utilizes ultralow magnetic field energy to

determine the exact place of the catheter within the left ventricle [57], allowing to achieve a real-time three dimensional map of the left ventricle. These maps can provide data about global left ventricular function (end-systolic, end-diastolic, stroke volumes, ejection fraction). The special sensor-tipped diagnostic catheter provides information of the local electrical activity, and the amplitude of this electric signal was shown to correlate well with the extent of myocardial ischemia [60]. The systematic acquisition of unipolar (UV), bipolar voltage (BV) and linear local shortening (LLS) data results in a three-dimensional map on the endocardial surface, which represents the left ventricle. Both the UV and BV value represent in vivo endocardial electrical signals, which could indicate myocardial viability. According to the definition of Kornowski et al., the LLS value "quantifies regional wall motion by calculating the fraction of linear distances of each endocardial point from its neighbouring points at end-systole, relative to end-diastolic distances" [22]. Decreased voltage and LLS values indicate myocardial necrosis. Both the global and the regional data provided by EMM were investigated in order to validate against other methods, including echocardiography [61], ventriculography [62, 63], scintigraphy [64-67], positron emission tomography [65, 67] and cMRI [68]. The evaluation of both viability (UV and BV) and regional wall motion abnormalities (LLS) could be performed side by side. As known from the previous literature FDG-PET could identify preserved metabolism, and therefore the areas of viable myocardium [69]. EMM is able to identify these regions as "electrically viable" myocardium, according to Koch et al [70]. According to these investigations the potential positive effect of revascularization could be estimated by the UV value, measured before percutaneous coronary intervention in patients, since the measured UV values exhibited good correlation with the recovery of regional wall motion assessed by ventriculography [70]. The parallel evaluation of voltage values and LLS could allow the detection of hibernated myocardium, which is indicated by preserved electrical and decreased LLS values [64]. Despite the above mentioned results regarding left ventricular function via EMM, especially the voltage and LLS values were not evaluated parallel by the regional cMRI data in reperfused and nonreperfused MI models.

4.2 Aims

In the second part, we determined the variables of global and regional left ventricular function via EMM and cMRI. The latter could serve as a gold standard both in measuring the variables of global and regional left ventricular function, while these characteristics of EMM were not evaluated in detail in different large animal MI models.

4.3 Methods

4.3.1 Electromechanical mapping procedure

After the previously delineated anaesthetical procedures and the induction of reperfused and nonreperfused MI (Chapter 3.4) EMM (NOGA, Biosense Webster, Cordis, Johnson and Johnson, Diamond Bar, CA) was performed on the sixth day, using 8F NOGA diagnostic catheter via left transfemoral approach. The mapping system consists of a triangular pad, inducing ultralow magnetic field, a reference catheter, a diagnostic catheter and a workstation, allowed both for online and offline data processing. All animals received 90 IU/kg unfractionated heparin before the mapping procedure. The diagnostic catheter was introduced retrogradely through the aortic valve into the left ventricle. The first points were acquired from the apex and the basis of the left ventricle using fluoroscopy, followed by systematic point acquisition process in the whole left ventricle, with a fill threshold of 15 mm. This approach allows the accurate detection of the apex to ensure the correct characterization of the maps using detailed segmentation of the left ventricle. The average duration of the mapping procedure was 60 minutes. Three dimensional colour-coded maps were derived in each animal, containing the values of UV, BV and LLS after the completion of the mapping procedure. The inner points and points located in the left atrium or recorded during ST elevation or without the standard eligibility criteria, as described by Gepstein et al. [71, 72] were deleted from the maps using visual assessment and moderate automated filtering processes. The maps of UV, BV and LLS values were analysed using the 12 segment bull's eye images, which were further divided into additional segments in order to be able to perform a more detailed comparison to the cMRI data. The

long axis of the left ventricle was divided into apex, midventricle and base consisting 20%, 40% and 40% of the long axis respectively. These parts were divided into four regions: anterior, septal, inferoposterior and lateral, each divided furthermore into two equal regions in the anterior, lateral and inferoposterior walls and into three equal regions of the septal wall (Figure 2.). The acquired images according to the different imaging modalities are demonstrated on Figure 3., the upper part represents one animal from the LAD balloon group, the lower part represents one animal from the Cx coil group. During the acquisition of endocardial points we did not experience any lethal complications; however the excessive manipulation, especially at the apex, and at the side of the infarcted and thinned myocardium could lead to perforation and pericardial tamponade formation. As a minor complication one animal evolved ventricular tachycardia in the LAD balloon group, and it was terminated by magnesium and beta-blocker administration.

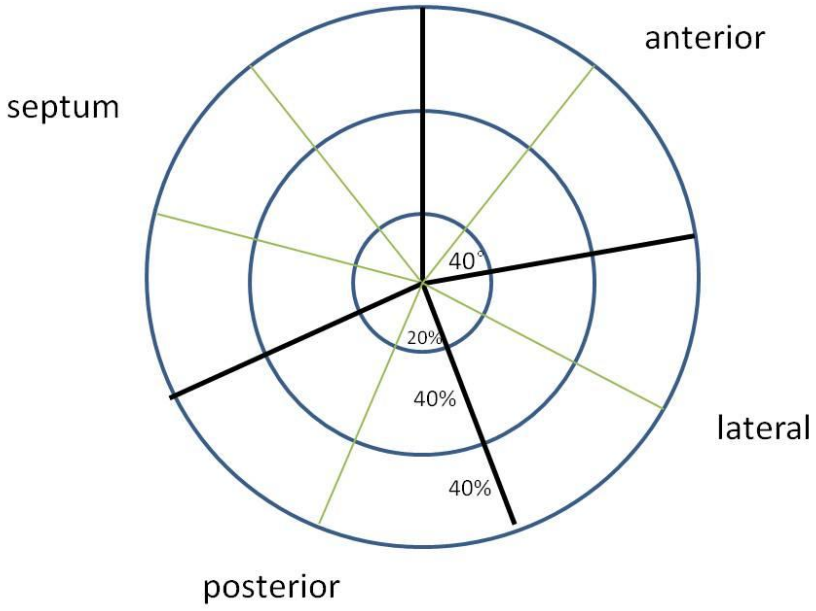

Figure 2. Bull's eye segmentation of the left ventricle for EMM and cMRI analysis, the apical, mid and basal part contains 9-9 segments.

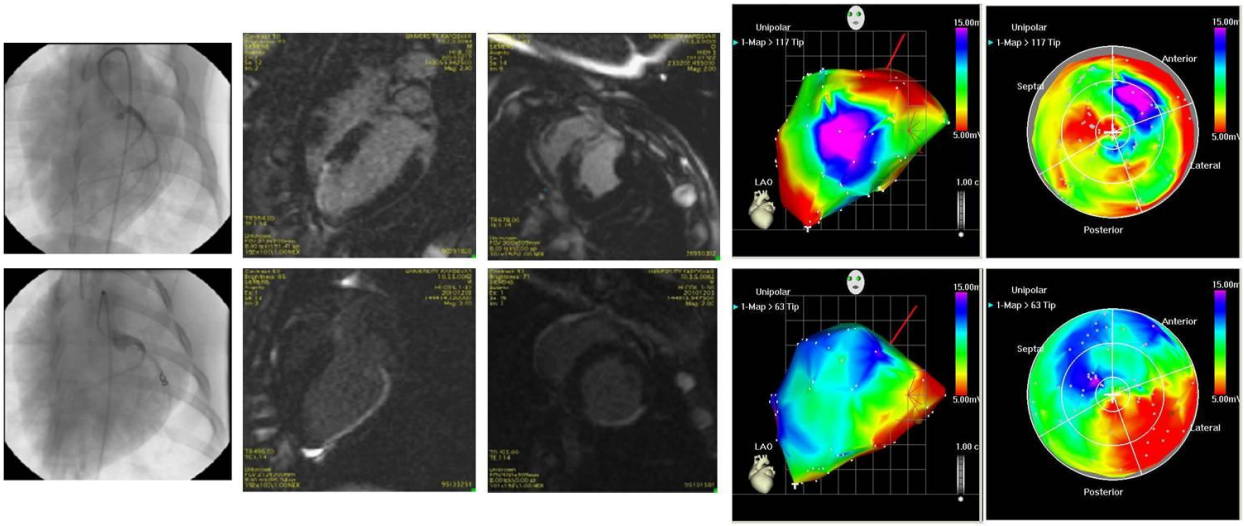

A B C

Figure 3. Demonstration of the infarct areas according to the different localizations
A: Coronary angiogram at the time of occlusion: balloon inflation in the LAD, coil deployment in the Cx
B: Long and short axis cMRI late enhancement images 10 minutes after contrast administration
C: EMM UV map, LAO and bull's eye view

4.3.2 Cardiac MRI acquisition and analysis

Cardiac MRI (Siemens, 1.5 T) was performed in anaesthetized animals in the supine position with electrocardiographic gating and breath-hold acquisitions, using flexible cardiac phased array coil, right after the EMM procedure. In order to improve the quality of images 100% oxygen was administered with positive pressure during the breath-hold acquisitions. For the late enhancement contrast images Gd(DTPA-BMA) (Omniscan) was administered 0.15 mmol/kg intravenously. If needed, the animals also received metoprolol 3 mg intravenously for heart rate control to enhance image quality. Short and long axis movie and delayed enhancement images were acquired following the basic scout imaging procedure 10 minutes after contrast injection. The acquisition parameters were the following: slice thickness 8 mm, field of view 300x206 mm, image resolution 256x192 pixels, flip angle 65 degrees, echo time 1.1 ms, repetition time 38.75 ms. Analysis regarding viability was captured on the short axis late enhancement images 10 minutes after

intravenous contrast administration (imaging parameters: slice thickness 8 mm, field of view 300x206 mm, image resolution: 192x132 mm, flip angle 50 degrees, echo time 1.14 ms, repetition time 465 ms). The inversion time was selected at each acquisition on the basis of the maximal zeroing of remote left ventricular myocardium. Cardiac MRI data were analysed using MASS software (Medis, NL), version 6.1.6. The epicardial and endocardial borders were defined in the end-systolic and end-diastolic phases of the short axis movie to capture data about the global left ventricular function (ejection fraction, stroke volume, end-diastolic volume, end-systolic volume). Detailed information was yielded about segmental end-systolic (ESWT) and diastolic wall thickness (EDWT) and regional wall motion characteristics via another derived value, wall thickening (WT, subtracting EDWT from ESWT, expressed as percentage of EDWT), using a 9 segment per slice model in order to be able to compare with the EMM data. The value of mean signal intensity (SI, au) and infarct transmurality (T%, as percentage of the whole wall thickness) was investigated using the same segmentation protocol on the acquired short axis late enhancement images. Increased signal intensity (late enhancement) represents infarcted areas. Full-width-half-maximum (FWHM) method was used to detect infarct size [73].

4.3.3. Statistical analysis

All results are presented as a mean ± standard error of mean (S.E.M.). Bland-Altman plots were reconstructed using MedCalc statistical software (version 12.3). The data regarding segmental derived wall motion parameters (EDWT, ESWT, WM and WT) and UV, BV, LLS were evaluated by Pearson correlation in a segment per segment fashion. For the statistical analysis SPSS software package, version 16.0 was used.

4.4 Results

4.4.1 EMM acquisition data

The average number of acquired EMM points was 138±30 per animal, during the on- and offline post processing analysis 38±19 and 24±7 points were deleted. The final number of eligible points was: 80±12. Segments containing less than two points were excluded from the evaluation; accordingly 166 segments (68.1%) were available for the statistical analysis.

4.4.2 Global left ventricular function and viability vs. EEM data

The average values of UV, BV, LLS, EMM and cMRI derived EF, EDV, ESV and SV are demonstrated in Table 1. The correlation between the EMM derived SV and the UV and BV values were significant (r=0.605, p=0.049, and r=0.671, p=0.024 respectively). The correlation was significant between the UV values and the EMM and cMRI derived EF (r=0.603, p=0.05; r=0.641, p=0.034 respectively). The correlation between the LLS values and the EMM derived EF also yielded significance (r=0.604, p=0.049). Furthermore the correlation between the average UV value and the left ventricular end-diastolic mass (LVmassED) was significant (r=0.755, p=0.007).

EMM data	UV (mV)	BV (mV)	LLS (%)	EF (%)	EDV (ml)	ESV (ml)	SV (ml)
LAD balloon	6.48±0.32	1.96±0.37	8.06±1.61	35.95±4.24	71.89±1.77	45.96±2.57	26.07±3.45
LAD coil	7.51±0.48	2.98±0.42	9.18±3.61	39.54±8.18	77.55±4.25	46.42±4.26	30.96±7.34
Cx coil	6.97±0.96	2.26±0.33	5.44±0.92	24±6.17	88.27±8.31	66.72±1.76	22.34±7.32

cMRI data	EF (%)	EDV (ml)	ESV (ml)	SV (ml)	Infarcted tissue (g)	Infarcted tissue (%)
LAD balloon	31.16±3.99	69.25±9.27	47.07±5.23	22.18±5.62	13.09±1.52	19.2±1.43
LAD coil	46.43±4.52	82.39±3.37	44.41±5.6	37.98±2.45	13.07±0.63	17.33±0.67
Cx coil	28.7±3.55	61.82±7.81	43.58±3.75	18.24±4.44	8.17±0.79	12.33±0.67

Table 1. The average values ± .S.E.M. of main variables in the EMM and cMRI data

There were no significant differences in the three groups regarding the absolute extent of myocardial infarcts. On the other hand the percentage of the infarcted area differed significantly in the LAD balloon (19.2±1.43%) and in the Cx coil group (12.33±0.67%) by one-way ANOVA and Tukey HSD post hoc test (LAD balloon vs. Cx coil, p=0.011).

The method of Bland-Altman analysis was used to display the average difference and limits of agreement between the cMRI values, as a reference and the EMM values (Figure 4.).

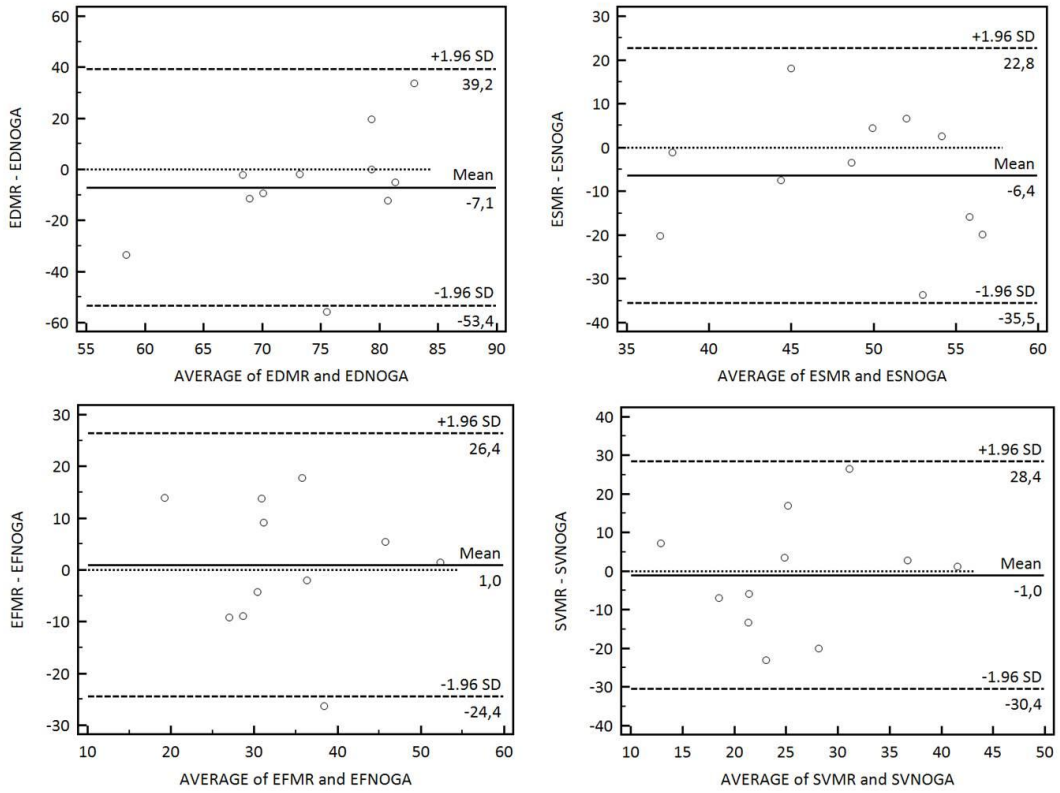

Figure 4. Bland-Altman plots of left ventricular EDV, ESV, EF, and SV derived from EMM and cMRI measurements from the LAD balloon, LAD coil and Cx coil groups.

4.4.3 Segmental wall motion and viability analysis

The relationship between the segmental average UV, BV and LLS values and EDWT, ESWT, WT and SI, T% was furthermore investigated. Data are demonstrated through the results of one animal in each group. The following

correlations were significant between the EMM derived (UV, BV, LLS) and cMRI derived (EDWT, ESWT, WT, SI and T%) values.

I. LAD balloon group: the correlation was significant between the segmental average UV value and the segmental average SI and T% value (r=-0.571, p=0.021 and r=-0.631, p=0.009, respectively). The segmental average BV value also showed good correlation with both viability parameters (r=-0.503, p=0.047 and r=-0.586, p=0.017), Figure 5.

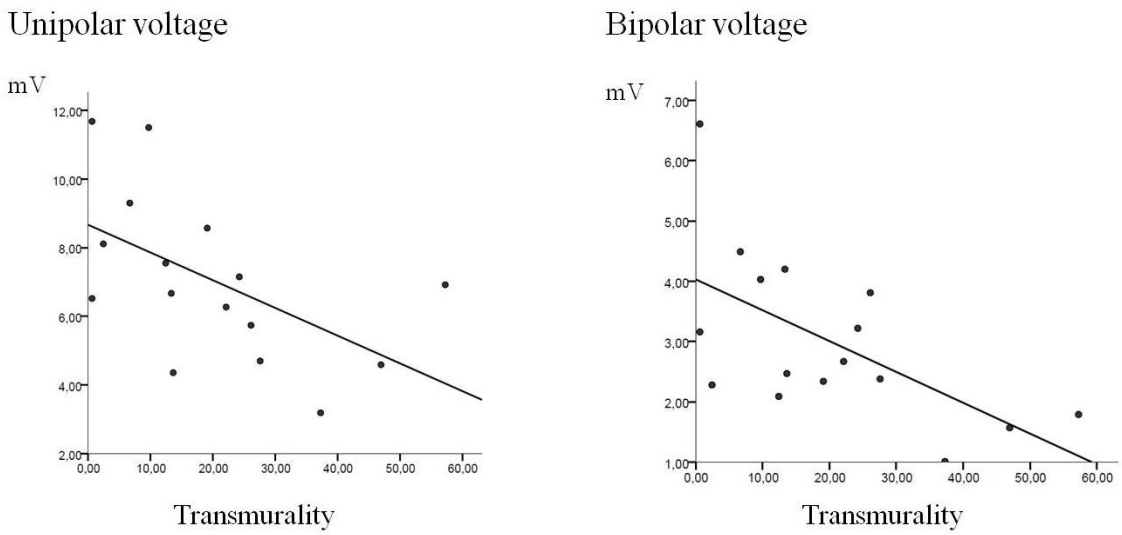

Figure 5. Correlation between segmental average UV, BV and T% in the LAD balloon group

II. LAD coil group: only the BV value exhibited statistically significant correlation with the segmental average SI value (r=-0.432, p=0.05).

III. Cx coil group: the average UV value also showed good correlation with the SI and T% values (r=-0.818, p <0.001, r=-0.778, p <0.001) and furthermore the relationship between the UV value and the EDWT and ESWT values was significant (r=0.782, p <0.001, r=0.694, p=0.003, Figure 6.).

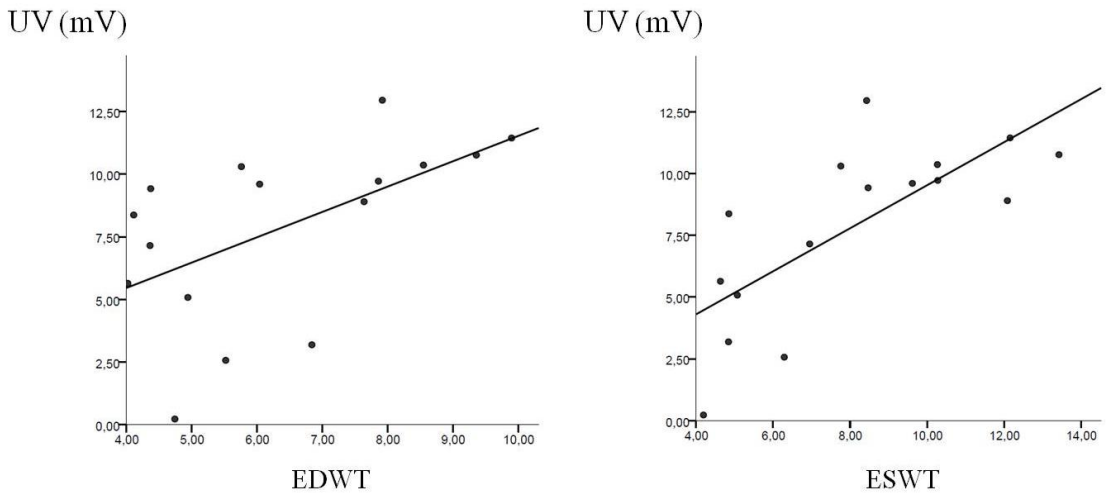

Figure 6. Correlation of average UV and EDWT, ESWT in the Cx coil group

4.5 Discussion

The agreement between the cMRI and EMM derived data concerning left ventricular function is moderate according to previous preclinical and clinical studies [62, 63, 70, 74-76]. In our study the EMM and cMRI derived values of global left ventricular function exhibited good agreement, but did not reached statistical significance in the correlational studies (data not shown). The main advantage of EMM is that it can be integrated to hemodynamical equipments and provides in vivo, online data about left ventricular global and regional function, without the significant increase of radiation dose. The large animal models allow investigating the electromechanical properties of animals with an extremely low EF with more increased scar tissue extent. The relationship between the global left ventricular parameters, especially between the EF, SV and the average UV values indicates a good diagnostic and may even prognostic impact of these parameters, since a more extended myocardial damage results in lower average voltage values [74, 77]. This could result from the mathematical average derived from both the viable and infarcted myocardial tissue; on the other hand it also could depend on left ventricular volume, wall thickness, degree of remodeling and extent of MI [77]. These factors affect remote areas outside the area of interest; therefore they influence the UV value, since it contains far-field components [78, 79]. The diagnostic accuracy of the LLS value highly depends on the homogeneity and number of points, and is derived

from the distances of the surrounding points in end-systole and end-diastole, partly neglecting the wall thickening during systole and is also influenced by passive motions of the heart [62, 79, 80]. In our study the LLS value showed moderate correlation with the left ventricular EF, and was not able to exhibit significant relationship with the regional EDWT, ESWT and WT values. The utilization of this parameter may be useful for the overall map analysis, and especially at the area of interest together with the voltage values, to identify discordant areas with preserved voltage and decreased LLS values. The regional left ventricular function can be characterized using the cMRI derived EDWT, ESWT and WT values, which are indicating the presence and progress of postinfarction remodeling. Our data suggests, that the UV and BV values may are also reflecting these processes properly. The segmental average voltage values exhibited good correlation with the average values of signal intensity and transmurality and furthermore this analysis served as a feedback, to prove the reliability of our data.

5. Evaluation of myocardial viability in porcine MI models

5.1 In vivo infarct quantification - imaging techniques

The exact quantification of the myocardial damage, e.g. the extent of necrotic tissue has high prognostic value and is a very crucial endpoint in preclinical studies; therefore several in vitro and in vivo methods were developed and used to fulfil this requirement. The earliest studies applied post-mortem histological investigations [3, 28, 81], changes in necroenzimes [19, 29], isometric contractile force using strain gauge technique [82] or measured regional wall thickening dynamics via ultrasonic crystals positioned on the walls of the left ventricle [83] and finally changes in electrocardiography [19] or local changes in temperature could also be measured [34]. The non-invasive imaging techniques could provide more exact quantification of the infarcted area, such as scintigraphy (SPECT) [84], positron emission tomography (PET) [85], computer tomography [86] or echocardiography [87] and furthermore could indicate reversible injuries also [88]. In the last decades cMRI has been proved to be a feasible and accurate non-invasive method for the detection and characterization of the infarcted and viable areas, and moreover has high prognostic value [89, 90]. The so called late or delayed enhancement phenomenon 10 minutes after intravenous injection of extracellular contrast materials (Gadolinium-diethylenetriamine pentaacetic acid - Gd-DTPA) indicates myocardial viability both in acute and healed MI and provides high localizational accuracy, regarding even the direct visualization of the transmural extent of MI [91, 92]. The background of this phenomenon is partly understood and in acute MI it could result from myocyte necrosis and consequent sarcomere membrane rupture, which prolongs the diffusion of contrast molecules [89], therefore the volume of distribution of Gd-DTPA increases. Extracellular contrast agents could overestimate the infarct size in the hyperacute stage of MI, although this phenomenon was not observed at eight weeks, which could be explained by the process of infarct shrinkage [92]. In the hyperacute phase the peripheral region represents a reversibly injured myocardium and produces transient enhancement, which resolves during the subacute stage. In the cases of chronic MI delayed enhancement could result from the delayed wash-in and wash-out kinetics of contrast agents in the scar tissue, and the increased volume of fibrotic

tissue [93]. This method was used frequently in several porcine MI studies and in our practice, as it is demonstrated in Figure 7.

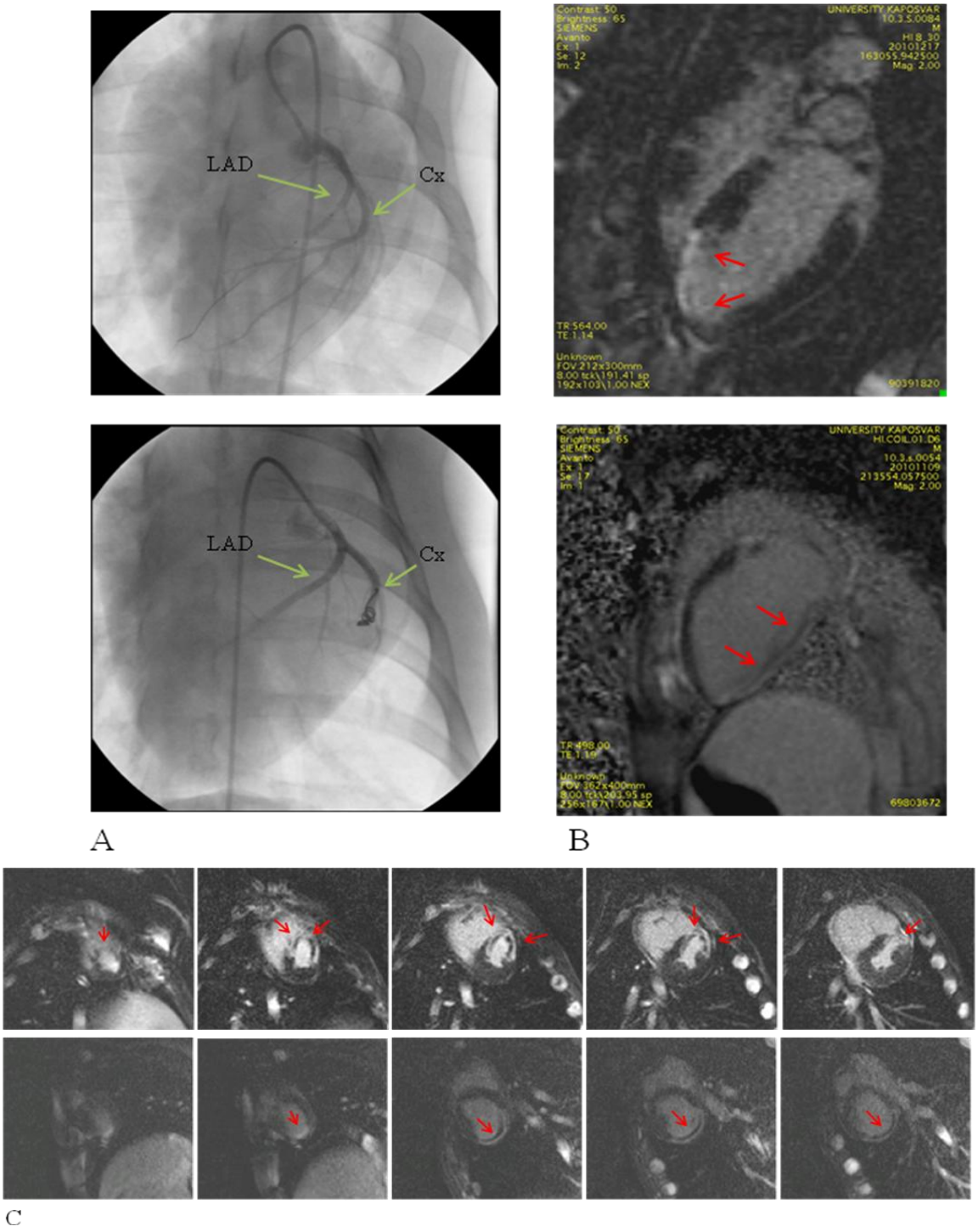

Figure 7. Cardiac MRI images of the infarct areas according to the different localization in porcine via the phenomenon of late enhancement imaging 10 minutes after contrast administration. All images were derived of one given animal from the group of balloon occlusion in the LAD and from the group of coil deployment in the Cx artery.

A: Coronary angiogram at the time of the coronary artery occlusion: balloon inflation in the LAD (upper image), coil deployment in the Cx (bottom image).
B: Long axis late enhancement images 10 minutes after contrast administration after the occlusion of the LAD (upper image, arrows indicate the late enhancement phenomenon in the septal and anterior wall) and the Cx artery (bottom image, arrows indicate the late enhancement phenomenon in the lateral and posterior wall).
C: Short axis late enhancement images 10 minutes after contrast administration. The upper sequence of pictures represents the consequent images of the left ventricle after balloon occlusion of the LAD. The bottom sequence of pictures represents the consequent images of the left ventricle after coil deployment in the Cx. (Arrows indicate the late enhancement phenomenon.)

Furthermore cMRI is the first non-invasive method that has the possibility to differentiate between reperfused and nonreperfused myocardial infarctions in the acute setting [94]. The recently developed combination of intravascular and extracellular Gadolinium-chelates raised the possibility to distinguish between acute and chronic MI [95] in open chest porcine models producing transient 120 min. occlusion of the LAD. Intravascular Gadolinium-chelates produce delayed contrast enhancement only in acute myocardial infarcts, due to the retain of intravascular contrast agents in the remodelled microvessels and the poor vascularisation and perfusion of scar tissues [96]. Also, recent studies of Kirschner et al. demonstrated also the value for the differentiation between acute and chronic infarcts in a closed chest, 180 minutes balloon occlusion model, since Gd(ABE-DTTA), which has intravascular properties and produces no delayed enhancement in chronic infarcts [97, 98].

The above mentioned properties of cMRI made it plausible to be the determinant of myocardial infarct size in animal studies [13, 99] and also raised the possibility of direct tracking stem cells after therapeutic interventions [100-102]. The measurement of infarct size is based on the extent of increased signal intensity; however several methods are available for the quantification of delayed enhancement images. From the above mentioned methods the utilization of the signal intensity percent infarct mapping beside the full-width-half-maximum method is accurate for infarct size quantification, and they were superior to remote plus standard deviation

thresholded late enhancement images for infarct size determination, validated against the gold standard triphenyl-tetrazolium-chloride (TTC) staining ex vivo [103]. Recently the signal intensity percent infarct mapping was also validated in vivo against remote plus standard deviation thresholded delayed enhancement images in vivo in a porcine closed chest balloon occlusion model and requires clinically acceptable scanning time [104]. In conclusion the utilization of cMRI in large animal models is accurate and could be feasible for follow-up studies, therefore decreases the necessary number of animals.

The availability of integrated magnetic resonance scanner within the catheterization laboratory is limited at this time; on the other hand the diagnostic procedures need to be accurate and fast, providing online data about myocardial viability. Recently EMM has been also utilized as an invasive, catheter-based method to measure myocardial viability and regional left ventricular function [22, 105]. The values of UV and BV allow determining the myocardial viability, raising even the possibility to gain information about the transmural extent of necrosis [68, 76]. The LLS value provides information about local regional contractility, therefore the infarcted areas are characterized by reduced values, and these values can be matched with the reduced voltage values [58]. The safety and feasibility of EMM has been proved in acut and chronic MI models to be able to identify and localize viable myocardial tissue and scar tissue [22, 58]. EMM has the unique opportunity, to be used directly in the catheterization laboratory, and also raised a unique way for local therapeutic approaches, e.g. administration of cells [106] or other biological materials [107, 108], and has been utilized for intramyocardial injections in several animal and clinical studies [109, 110].

5.2 Aims

The intramyocardial injection of cells or growth factors is the unique and main advantage of EMM. This feature requires the exact determination of the necrotic area, the transitional zone and viable tissue. Cardiac MRI serves as a gold standard regarding myocardial viability among the non-invasive methods due to its high spatial resolution, concerning especially the transmural extent of necrosis. The diagnostic features of EMM were investigated in accordance to the results of cMRI regarding myocardial viability.

5.3 Methods

The design of experiments and the methods, utilized during the evaluation of myocardial viability are reviewed in Chapter 3.4, 4.3.2 and 4.3.1. Briefly, six days after the induction of MI, via balloon occlusion or coil deployment in the LAD, or coil deployment in the Cx, cMRI and EMM examinations were carried out. The late enhancement phenomenon indicating the presence and transmural extent of nonviable tissue were evaluated according to the above described segmentation protocol (Figure 2.) 10 minutes after contrast administration. During the EMM procedure the values of BV and UV represented the presence or absence of viable tissue, since the measurement of low voltage values indicates scar tissue. The values of LLS were also evaluated, presenting the characteristics of local wall motion. The same segmentation protocol was used as described above to be able to perform a segment by segment analysis.

5.3.1. Statistical analysis

All results are presented as a mean ± standard error of mean (S.E.M.). Data regarding segmental voltage and LLS values were grouped according to the cMRI viability data into three groups, segments containing transmural late enhancement (increased signal intensity more than 50 % of the whole wall thickness), subendocardial late enhancement (increased signal intensity in less than 50 % of the whole wall thickness) and viable tissue (absence of increased signal intensity). These groups were analysed by one-way analysis of variance (one-way ANOVA) and the Tukey HSD test was employed for post hoc comparison. Receiver operator characteristic (ROC) analyses were used for the determination of the predictive value of EMM parameters compared to the cMRI acquisition. The p value of less than 0.05 was considered statistically significant at each analysis. For the statistical analysis SPSS software package, version 16.0 was used.

5.4 Results

5.4.1 Transmural distribution of scar area

The segmental average UV, BV and LLS values were grouped according to the cMRI transmurality data as segments containing transmural, subendocardial late enhancement or viable tissue. After the evaluation using one-way ANOVA, which showed significant difference between the three groups, Tukey HSD post hoc tests were carried out, which yielded significantly decreased UV and BV values in the segments with transmural and subendocardial late enhancement than in the viable areas, and significantly decreased LLS values in the segments with transmural late enhancement, than in viable segments as demonstrated in Fig. 8A.

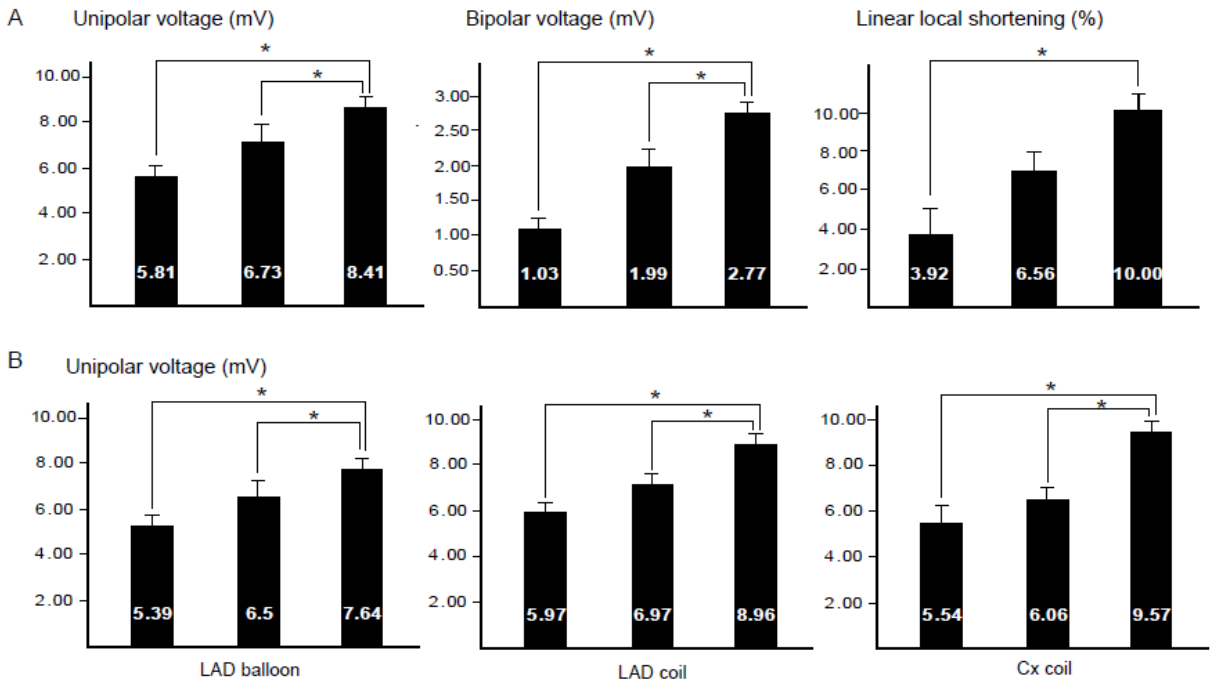

Figure. 8.

A: Grouped analysis using one-way ANOVA and Tukey HSD post hoc test of the UV, BV and LLS segmental average values using the overall data, * indicates p values <0.05, bars represent the average values of UV, BV and LLS of segments characterized by transmural, subendocardial late enhancement or viable myocardial tissue on cMRI images, respectively.

B: Grouped analysis using one-way ANOVA and Tukey HSD post hoc test of the UV, segmental average values in the three animal groups, * indicates p values <0.05, bars represent the average values of UV values of segments characterized by transmural, subendocardial late enhancement or viable myocardial tissue on cMRI images, respectively.

We also performed one-way ANOVA tests according the three animal groups, the results are summarized in Table 2., and Figure 8B. Segments with subendocardial and transmural late enhancement had significantly less UV values, than the viable segments in all groups. In the case of the BV value this phenomenon was only present in the LAD balloon group.

		Viable tissue	Subendocardial late enhancement	Transmural late enhancement
UV (mV)		8.41±0.27	6.73±0.33 *	5.81±0.28 *
BV (mV)		2.77±0.19	1.99±0.18 *	1.03±0.16 *
LLS (%)		10±0.83	6.56±1.31	3.92±1.73 *
UV (mV)	LAD balloon	7.64±0.33	6.5±0.26 *	5.39±0.32 *
	LAD coil	8.96±0.56	6.97±0.46 *	5.97±0.5 *
	Cx coil	9.57±0.53	6.06±0.61 *	5.54±1.07 *
BV (mV)	LAD balloon	2.2±0.26	1.76±0.24	0.7±0.13 *
	LAD coil	3.65±0.39	2.42±0.35	1.36±0.28 *
	Cx coil	2.8±0.35	1.82±0.3	1.68±0.8 *

Table 2. One-way ANOVA according to the overall data from all animal groups (upper third part), and the UV and BV values of the LAD balloon, LAD coil and Cx coil groups, * indicates p<0.05, in cases of viable tissue vs. transmural late enhancement, and viable tissue vs. subendocardial late enhancement.

5.4.2 ROC analysis of cMRI and EMM data

Cardiac MRI for determining myocardial viability is a well tested gold standard method. We investigated the indicative capacity of the segmental average UV, BV and LLS values against cMRI segmental average signal intensity and transmurality using ROC analysis. First we examined the indicative value of UV, BV and LLS overall in the three animal group. The ROC curves were constructed to compare the subendocardial late enhancement vs. viable tissue and transmural late enhancement vs. viable tissue. The results are summarized in Figure 9. and Table 3. The AUC for the UV value was 0.657 ($p=0.007$), 0.783 ($p<0.001$), for the comparison of subendocardial and transmural late enhancement with normal tissue, for the BV value AUC was 0.551 ($p=0.378$), 0.824 ($p<0.001$), for the same diagnostic settings, respectively.

Subendocardial late enhancement vs. normal tissue

	AUC	**95% CI**	**SEM**	**P value**
UV	**0.657**	**0.552-0.763**	**0.054**	***0.007***
BV	**0.551**	**0.442-0.661**	**0.056**	**0.378**
LLS	**0.623**	**0.515-0.731**	**0.055**	***0.035***

Transmural late enhancement vs. normal tissue

	AUC	**95% CI**	**SEM**	**P value**
UV	**0.783**	**0.704-0.861**	**0.04**	***<0.001***
BV	**0.824**	**0.749-0.9**	**0.038**	***<0.001***
LLS	**0.642**	**0.534-0.750**	**0.05**	***0.009***

Table 3. Main parameters of the ROC curves

Subendocardial late enhancement vs. viable tissue Transmural late enhancement vs. viable tissue

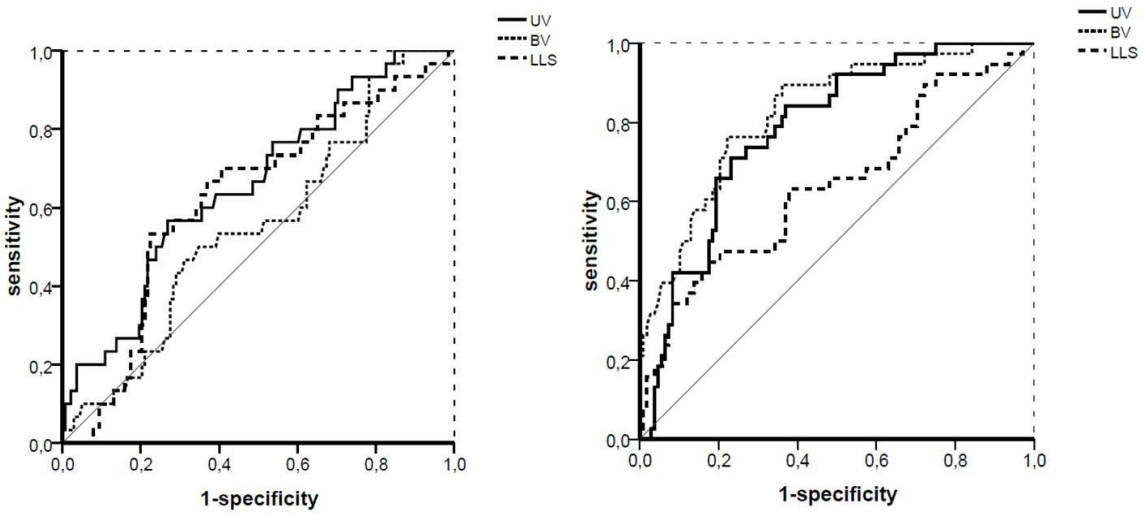

Figure 9. ROC curves from the overall data of all animal groups

We also evaluated the possible differences between the accuracy regarding the two distinct infarct areas, namely at the territory of the LAD and Cx using ROC curve analysis. The characteristics of the ROC curve are summarized in Table 4. and Figure 10. The AUC for the UV value was 0.691 (p=0.037), 0.809 (p=0.002), in the LAD balloon and coil groups and 0.855 (p<0.001), 0.864 (p=0.001) in the Cx coil group for the subendocardial and transmural late enhancement vs. normal tissue, respectively. The BV value also expressed good diagnostic accuracy in the LAD balloon and coil group (subendocardial scar vs. normal tissue AUC=0.687, p=0.041, transmural late enhancement vs. normal tissue AUC=0.853, p<0.001), and failed to demonstrate significant diagnostic efficacy in the Cx coil group.

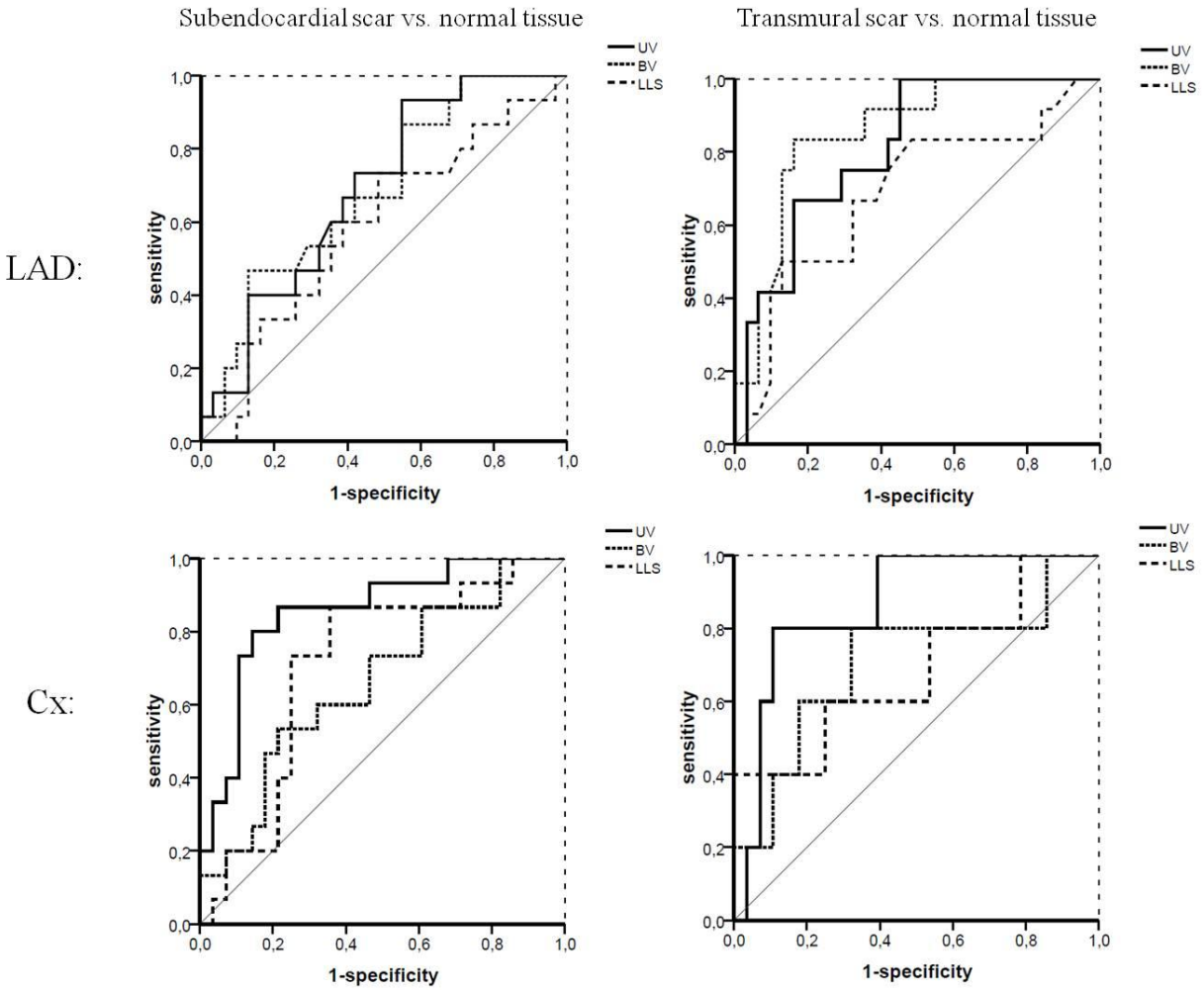

Figure 10. Detailed ROC analysis, according the different infarct areas using the segmental average UV, BV, LLS values

Subendocardial late enhancement vs. normal tissue

		AUC	95% CI	SEM	P value
LAD	UV	0.691	0.538-0.845	0.082	*0.037*
	BV	0.687	0.534-0.816	0.082	*0.041*
	LLS	0.588	0.412-0.764	0.09	0.337
Cx	UV	0.855	0.714-0.943	0.061	*<0.001*
	BV	0.662	0.491-0.833	0.087	0.083
	LLS	0.71	0.547-0.872	0.083	0.055

Transmural late enhancement vs. normal tissue

		AUC	95% CI	SEM	P value
LAD	UV	0.809	0.66-0.913	0.068	*0.002*
	BV	0.853	0.713-0.943	0.062	*<0.001*
	LLS	0.685	0.499-0.872	0.095	0.062
Cx	UV	0.864	0.716-1.013	0.076	*<0.001*
	BV	0.707	0.427-0.987	0.143	0.145
	LLS	0.686	0.401-0.971	0.145	0.192

Table 4. Main characteristics of the ROC curves of different territories

5.5 Discussion

The UV value was significantly decreased in segments containing subendocardial or transmural scar tissue according to our results, and this phenomenon was reproducible in different localizations also. During the ROC analysis the UV value provided good diagnostic accuracy and this result also seemed to be independent of the localization of the infarcted area. Although the 17-segment model is widely used and accepted in the human cMRI diagnostics, [111] the detailed segmentation allowed to perform a more detailed analysis in all animals. The basal, mid- and apical region of the heart was tested equally in 9-9 segments, and this model allowed minimizing misalignments during the anatomical matching to the cMRI images. All analyses were performed using this segmentational protocol. The number of segments with eligible number of points were 68,1%, this factor may influenced our data, on the other hand in case of the 12 segment model we only had to exclude 12 segments (8,3%), and similarly the number of acquired and eligible points were consistent with other data [61]. Despite the slight overestimation of the infarct area by delayed enhancement cMRI imaging, it was feasible for the segmental comparison, as a widely accepted and used method for myocardial viability [89, 92]. Myocardial segments characterized by 50% or less extent of hyperenhancement on delayed enhancement cMRI were termed as segments with subendocardial scar tissue in our porcine model. This classification was widely used in previous clinical assessments of EMM [68, 76], and this value predicts properly the positive effect after planned revascularization procedures [90]. Wolf et al. demonstrated good discriminative capacity of BV value in a dog model of MI with different transmurality using histopathological analysis, our results also demonstrate this discriminative capacity for the UV and BV value, on the other hand we used a less detailed characterization for the transmurality (50-100%, 50-0% or viable tissue), but in a more detailed segmental distribution of the whole left ventricle [105]. The present study demonstrates this significant discriminative capacity of EMM both in the LAD balloon and LAD coil groups for the UV value.

The main aim of ROC analysis was to investigate the differences in the diagnostic efficacy of EMM, variables in different localizations, especially when the posterobasal region is involved in the infarct evolution as it was already described in several papers [22, 64, 67, 70, 112]. Overall the diagnostic efficacy was more

pronounced in cases of differentiating between transmural late enhancement and viable areas, but yielded similarly significant AUC values in the detection of subendocardial late enhancement for the UV value. We demonstrated good diagnostic efficacy for both the UV and BV values in animals with infarction on the LAD territory, and the UV value exhibited good efficacy in the Cx coil group also. On the other hand the diagnostic efficacy of the BV value disappeared in the Cx coil group, as the AUC values did not appeared statistically significant. In this study the accuracy of the UV value was more pronounced than the accuracy of the BV value. The UV value is influenced by contact stability and far field electrical potentials, the BV value depends from the orientation of the tip electrode on the endocardial surface, this latter fact may increase the number of false positive points [22, 58]. One further explanation for this phenomenon could be the greater variability of BV values, reported by Fallavollita et al. [79], however our study was carried in the acute setting of MI. Interestingly the relationship between the UV value and the LvmassED was significant (as mentioned in Chapter 4.4.2) and the correlation between the UV value and the wall thickness values were also significant (Chapter 3.3.3) in the segmental analysis, so these data supports the better utility of the UV value in this setting and this is could be a consequence of the above mentioned influencing role of far field potentials. The diagnostic accuracy of the LLS value highly depends on the homogeneity and number of points as it was emphasized in the previous discussion, therefore it did not identify correctly the presence or absence of the infarcted area. [62, 79, 80].

In conclusion, EMM indicated accurately the presence and location of the infarcted area both in the reperfused and nonreperfused MI model. The EMM derived UV values showed good correlation with the global left ventricular function, and regional viability data and indicated properly the presence of subendocardial and transmural late enhancement regardless of pathomechanism and localization. ROC analysis revealed good diagnostic accuracy for the UV value regarding the different localization of MI. The main advantage of EMM is the potential and prompt availability in the catheterization laboratory, as a reliable method for myocardial viability measurements regardless of the pathomechanism and location of MI. This study proves the diagnostic efficacy of EMM in different clinical settings therefore could improve the clinical utilization of this method, especially in cases where treatment was not initiated within the desired time range e.g. in late comers, since the

main scope of studies regarding the utilization of EMM is the unique possibility of intramyocardial therapeutic administration of drugs or biological materials on a minimal invasive way to improve left ventricular function.

6. Novel findings

Our results outline the investigations of myocardial infarcts with different pathomechanism (reperfused or nonreperfused) and localization (LAD or Cx) using EMM first time to our knowledge.

The detailed type of segmentation, which was applied in the analysis of both cMRI and EMM allows accurate interpretation of the results.

The UV voltage value exhibited good correlation with the segmental average signal intensity values and the value of infarct transmurality, which also indicates the role in the differentiation between viable and nonviable tissue.

The EMM derived UV value was able to detect infarct areas characterized by low voltage values in the reperfused and similarly in the nonreperfused MI model.

The UV value could indicate the presence of nonviable tissue, which was independent from the localization of MI.

7. Appendix

Summary of the different closed chest techniques for MI induction from the aspect of mortality, VF, reperfusion, and infarct size measurements

Authors	Method	Nr. of animals	Mortality rate	Infarct size measuring method	Reperfusion	Rate of VF
Capone et al., 1975	Balloon occlusion LAD	15	n.a.	ST segment elevation	No reperfusion	n.a.
Kren et al., 2010	Balloon occlusion LAD	4	n.a.	Only qualitative histological analysis	After 90 min. occlusion	n.a.
Krombach et al., 2005	Balloon occlusion LAD	44	22,73%	TTC staining Reperfused: 15,8± 5,1% Nonreperfused: 21,5±8,7%	After 45 min. occlusion/no reperfusion	59,1%
Perez de Prado et al., 2009	Balloon occlusion LAD	15	33%	Histology (HE and Masson trichrome) 20,4±4,3%	After 75 min. occlsuion	87%
Saeed et al., 2010	Balloon occlusion LAD	18	22,22%	Three days after induction MR infarct size: 15,5±0,7% TTC staining: 15,0±1%	After 90 min. occlusion	n.a.
Suzuki et al., 2007	Balloon occlusion LAD	78	20,51%	TTC staining 7days after induction 60 min proximal LAD occl.: 18,3±1,4% 30 min proximal LAD occl.: 5,8±6,6% 60 min mid LAD occl.: 13±1,4%	After 30 or 60 min. occlusion	40%
Dib et al., 2006	Coil deployment LAD	44	20,45%	Histology: 14,2±2,9%	No reperfusion	13,6%
Peukert et al., 2009	Coil deployment Cx	20	25% (overall: 35%)	Two days after induction MR infarct size: 4,4±2,3 cm^3 TTC staining: 4,3±2,2 cm^3	No reperfusion	45%

Uriuda et al., 1997	Coil deployment LAD	40	n.a.	Open/closed chest lysis with rt-PA, TTC staining: 13±8 / 15±5%	Lysis with rt-PA	15%
Abegunewardene et al., 2009	Balloon occlusion/ thrombin injection LAD	27	48,15%	Eight weeks after induction MR infarct size: 30 min occlusion: 5,3±5,4% 45 min. occlusion: 9,7±3,4% No reperfusion: 16,9±2,1%	After 30 or 45 min. occlusion/no reperfusion	44,44%
Eldar et al., 1994	Injection of agarose gel microbeads LAD	11	36,36%	Epicardial infarct area: 8,8±5% (11-32% of the left ventricular surface)	No reperfusion	n.a.
Naslund et al., 1990	injection of a 2 mm ball into LAD or Cx or RCA. Reperfusion was achieved by retraction of the ball via an attached filament	78	6,5%	TTC staining (expressed as infarct weight as % of myocardium at risk) 30 min. occlusion: 6,72±2,51% 60 min. occlusion: 8,21±2,56% 90 min. occlusion: 9,25±2,5%	After 30, 60 or 90 min. occlusion	15,9%
Agress et al., 1952	Coronary embolization with graded microspheres	49	34,7%	n.a.	No reperfusion	28,57%
Salazar et al., 1961	Endothelial electrical injury in the LAD or Cx	23	0%	n.a.	No reperfusion	n.a.
Reffelmann et al.,2003	Foam sponge deployment in the Cx (LAD)	21	38%	n.a.	No reperfusion	76,2% (VT and VF)

7. References:

1. Roger, V.L., et al., *Trends in incidence, severity, and outcome of hospitalized myocardial infarction.* Circulation, 2010. **121**(7): p. 863-9.
2. Pfeffer, M.A. and E. Braunwald, *Ventricular remodeling after myocardial infarction. Experimental observations and clinical implications.* Circulation, 1990. **81**(4): p. 1161-72.
3. Reimer, K.A., et al., *The wavefront phenomenon of ischemic cell death. 1. Myocardial infarct size vs duration of coronary occlusion in dogs.* Circulation, 1977. **56**(5): p. 786-94.
4. Kim, C.B. and E. Braunwald, *Potential benefits of late reperfusion of infarcted myocardium. The open artery hypothesis.* Circulation, 1993. **88**(5 Pt 1): p. 2426-36.
5. Blumgart, H.L., et al., *The experimental production of intercoronary arterial anastomoses and their functional significance.* Circulation, 1950. **1**(1): p. 10-27.
6. Crick, S.J., et al., *Anatomy of the pig heart: comparisons with normal human cardiac structure.* J Anat, 1998. **193 (Pt 1)**: p. 105-19.
7. Weaver, M.E., et al., *A quantitative study of the anatomy and distribution of coronary arteries in swine in comparison with other animals and man.* Cardiovasc Res, 1986. **20**(12): p. 907-17.
8. Maxwell, M.P., D.J. Hearse, and D.M. Yellon, *Species variation in the coronary collateral circulation during regional myocardial ischaemia: a critical determinant of the rate of evolution and extent of myocardial infarction.* Cardiovasc Res, 1987. **21**(10): p. 737-46.
9. Hearse, D.J. and F.J. Sutherland, *Experimental models for the study of cardiovascular function and disease.* Pharmacol Res, 2000. **41**(6): p. 597-603.
10. Verdouw, P.D., et al., *Animal models in the study of myocardial ischaemia and ischaemic syndromes.* Cardiovasc Res, 1998. **39**(1): p. 121-35.
11. Naslund, U., et al., *A closed-chest myocardial occlusion-reperfusion model in the pig: techniques, morbidity and mortality.* Eur Heart J, 1992. **13**(9): p. 1282-9.

12. Bitkover, C.Y., et al., *Effects of cardiac surgery on some clinically used inflammation markers and procalcitonin.* Scand Cardiovasc J, 2000. **34**(3): p. 307-14.
13. Peukert, D., et al., *A minimally invasive method for induction of myocardial infarction in an animal model using tungsten spirals.* Int J Cardiovasc Imaging, 2009. **25**(5): p. 529-35.
14. Hosenpud, J.D., N.N. Yung, and M.J. Morton, *Left ventricular pressure-volume relations shift to the left after long-term loss of pericardial restraint.* Circulation, 1983. **68**(1): p. 155-63.
15. Abendschein, D.R., W.A. Tacker, Jr., and C.F. Babbs, *Protection of ischemic myocardium by whole-body hypothermia after coronary artery occlusion in dogs.* Am Heart J, 1978. **96**(6): p. 772-80.
16. Duncker, D.J., et al., *Effect of temperature on myocardial infarction in swine.* Am J Physiol, 1996. **270**(4 Pt 2): p. H1189-99.
17. Garcia-Dorado, D., et al., *Myocardial reperfusion in the pig heart model: infarct size and duration of coronary occlusion.* Cardiovasc Res, 1987. **21**(7): p. 537-44.
18. Bush, L.R., et al., *Effect of diltiazem on extent of ultimate myocardial injury resulting from temporary coronary artery occlusion in dogs.* J Cardiovasc Pharmacol, 1982. **4**(2): p. 285-96.
19. Maroko, P.R., et al., *Factors influencing infarct size following experimental coronary artery occlusions.* Circulation, 1971. **43**(1): p. 67-82.
20. Kloner, R.A., *Does reperfusion injury exist in humans?* J Am Coll Cardiol, 1993. **21**(2): p. 537-45.
21. Thygesen, K., J.S. Alpert, and H.D. White, *Universal definition of myocardial infarction.* Eur Heart J, 2007. **28**(20): p. 2525-38.
22. Kornowski, R., et al., *Preliminary animal and clinical experiences using an electromechanical endocardial mapping procedure to distinguish infarcted from healthy myocardium.* Circulation, 1998. **98**(11): p. 1116-24.
23. Capone, R.J., A.S. Most, and P.A. Sydik, *Precordial ST segment mapping. A sensitive technique for the evaluation of myocardial injury?* Chest, 1975. **67**(5): p. 577-82.
24. Kren, L., et al., *Experimental model of myocardial infarction: Histopathology and reperfusion damage revisited.* Pathol Res Pract, 2010. **206**(9): p. 647-50.

25. Krombach, G.A., et al., *Minimally invasive close-chest method for creating reperfused or occlusive myocardial infarction in swine.* Invest Radiol, 2005. **40**(1): p. 14-8.
26. Perez de Prado, A., et al., *Closed-chest experimental porcine model of acute myocardial infarction-reperfusion.* J Pharmacol Toxicol Methods, 2009. **60**(3): p. 301-6.
27. Saeed, M., et al., *Noninvasive MR characterization of structural and functional components of reperfused infarct.* Acta Radiol, 2010. **51**(10): p. 1093-102.
28. Harris, A.S., *Delayed development of ventricular ectopic rhythms following experimental coronary occlusion.* Circulation, 1950. **1**(6): p. 1318-28.
29. Shell, W.E., J.K. Kjekshus, and B.E. Sobel, *Quantitative assessment of the extent of myocardial infarction in the conscious dog by means of analysis of serial changes in serum creatine phosphokinase activity.* J Clin Invest, 1971. **50**(12): p. 2614-25.
30. Jacobson, E.D. and K.G. Swan, *Hydraulic occluder for chronic electromagnetic blood flow determinations.* J Appl Physiol, 1966. **21**(4): p. 1400-2.
31. Khouri, E.M. and D.E. Gregg, *An inflatable cuff for zero determination in blood flow studies.* J Appl Physiol, 1967. **23**(3): p. 395-7.
32. Tennant, R., *Studies in the Pathology of Vascular disease: Studies on Experimental Coronary Occlusion.* Yale J Biol Med, 1936. **9**(1): p. 60-64 8.
33. Schulz, R., et al., *Ischemic preconditioning in pigs: a graded phenomenon: its relation to adenosine and bradykinin.* Circulation, 1998. **98**(10): p. 1022-9.
34. Papp, L., et al., *Natural history of acute regional myocardial ischaemia revealed by infrared thermography in the canine heart.* Acta Morphol Hung, 1985. **33**(1-2): p. 123-42.
35. Jiga, L.P., et al., *Thoracoscopic approach of the internal mammary artery (IMA): a training model in pigs.* Microsurgery, 2008. **28**(5): p. 375-9.
36. Suzuki, Y., et al., *In vivo porcine model of reperfused myocardial infarction: in situ double staining to measure precise infarct area/area at risk.* Catheter Cardiovasc Interv, 2008. **71**(1): p. 100-7.

37. Naslund, U., et al., *Effects of reperfusion and superoxide dismutase on myocardial infarct size in a closed chest pig model.* Cardiovasc Res, 1992. **26**(2): p. 170-8.
38. Agress, C.M., et al., *Protracted shock in the closed-chest dog following coronary embolization with graded microspheres.* Am J Physiol, 1952. **170**(3): p. 536-49.
39. Kordenat, R.K., P. Kezdi, and E.L. Stanley, *A new catheter technique for producing experimental coronary thrombosis and selective coronary visualization.* Am Heart J, 1972. **83**(3): p. 360-4.
40. Dib, N., et al., *A percutaneous swine model of myocardial infarction.* J Pharmacol Toxicol Methods, 2006. **53**(3): p. 256-63.
41. Gavira, J.J., et al., *A comparison between percutaneous and surgical transplantation of autologous skeletal myoblasts in a swine model of chronic myocardial infarction.* Cardiovasc Res, 2006. **71**(4): p. 744-53.
42. Reffelmann, T., et al., *A novel minimal-invasive model of chronic myocardial infarction in swine.* Coron Artery Dis, 2004. **15**(1): p. 7-12.
43. Eldar, M., et al., *A closed-chest pig model of sustained ventricular tachycardia.* Pacing Clin Electrophysiol, 1994. **17**(10): p. 1603-9.
44. Salazar, A.E., *Experimental myocardial infarction. Induction of coronary thrombosis in the intact closed-chest dog.* Circ Res, 1961. **9**: p. 1351-6.
45. Helmius, G., *Myocardial infarction without coronary occlusion. A study with a new experimental method in sheep.* Ups J Med Sci Suppl, 1980. **29**: p. 1-28.
46. Gerber, B.L., et al., *Microvascular obstruction and left ventricular remodeling early after acute myocardial infarction.* Circulation, 2000. **101**(23): p. 2734-41.
47. Wu, K.C., et al., *Prognostic significance of microvascular obstruction by magnetic resonance imaging in patients with acute myocardial infarction.* Circulation, 1998. **97**(8): p. 765-72.
48. Uriuda, Y., et al., *Coronary thrombosis/thrombolysis in pigs: effects of heparin, ASA, and the thrombin inhibitor inogatran.* J Pharmacol Toxicol Methods, 1998. **39**(2): p. 81-9.
49. van der Spoel, T.I., et al., *Human relevance of pre-clinical studies in stem cell therapy: systematic review and meta-analysis of large animal models of ischaemic heart disease.* Cardiovasc Res, 2011.

50. Abegunewardene, N., et al., *Usefulness of MRI to differentiate between temporary and long-term coronary artery occlusion in a minimally invasive model of experimental myocardial infarction.* Cardiovasc Intervent Radiol, 2009. **32**(5): p. 1033-41.
51. Huang, Z., et al., *Ligating LAD with its whole length rather than diagonal branches as coordinates is more advisable in establishing stable myocardial infarction model of swine.* Exp Anim, 2010. **59**(4): p. 431-9.
52. White, H.D., et al., *Left ventricular end-systolic volume as the major determinant of survival after recovery from myocardial infarction.* Circulation, 1987. **76**(1): p. 44-51.
53. Matthaei, D., et al., *Regional physiological functions depicted by sequences of rapid magnetic resonance images.* Lancet, 1985. **2**(8460): p. 893.
54. Baer, F.M., et al., *[Magnetic resonance tomography imaging techniques for diagnosing myocardial vitality]*. Herz, 1994. **19**(1): p. 51-64.
55. Bellenger, N.G., et al., *Comparison of left ventricular ejection fraction and volumes in heart failure by echocardiography, radionuclide ventriculography and cardiovascular magnetic resonance; are they interchangeable?* Eur Heart J, 2000. **21**(16): p. 1387-96.
56. van der Spoel, T.I., et al., *Human relevance of pre-clinical studies in stem cell therapy: systematic review and meta-analysis of large animal models of ischaemic heart disease.* Cardiovasc Res, 2011. **91**(4): p. 649-58.
57. Ben-Haim, S.A., et al., *Nonfluoroscopic, in vivo navigation and mapping technology.* Nat Med, 1996. **2**(12): p. 1393-5.
58. Gepstein, L., et al., *Electromechanical characterization of chronic myocardial infarction in the canine coronary occlusion model.* Circulation, 1998. **98**(19): p. 2055-64.
59. Psaltis, P.J., et al., *Assessment of myocardial fibrosis by endoventricular electromechanical mapping in experimental nonischemic cardiomyopathy.* Int J Cardiovasc Imaging, 2010. **27**(1): p. 25-37.
60. Ruffy, R., et al., *Relationship between changes in left ventricular bipolar electrograms and regional myocardial blood flow during acute coronary artery occlusion in the dog.* Circ Res, 1979. **45**(6): p. 764-70.

61. Lessick, J., et al., *Evaluation of inotropic changes in ventricular function by NOGA mapping: comparison with echocardiography.* J Appl Physiol, 2002. **93**(2): p. 418-26.
62. Sarmento-Leite, R., et al., *Comparison of left ventricular electromechanical mapping and left ventricular angiography: defining practical standards for analysis of NOGA maps.* Tex Heart Inst J, 2003. **30**(1): p. 19-26.
63. Tan, E.S., et al., *Evaluation of global left ventricular function assessment of non-fluorescent electromechanical endocardial mapping compared with biplane left ventricular contrast angiography.* Neth Heart J, 2010. **18**(2): p. 72-7.
64. Gyongyosi, M., et al., *Online myocardial viability assessment in the catheterization laboratory via NOGA electroanatomic mapping: Quantitative comparison with thallium-201 uptake.* Circulation, 2001. **104**(9): p. 1005-11.
65. Wiggers, H., et al., *Electromechanical mapping versus positron emission tomography and single photon emission computed tomography for the detection of myocardial viability in patients with ischemic cardiomyopathy.* J Am Coll Cardiol, 2003. **41**(5): p. 843-8.
66. Gyongyosi, M., et al., *Characterization of hibernating myocardium with NOGA electroanatomic endocardial mapping.* Am J Cardiol, 2005. **95**(6): p. 722-8.
67. Graf, S., et al., *Electromechanical properties of perfusion/metabolism mismatch: comparison of nonfluoroscopic electroanatomic mapping with 18F-FDG PET.* J Nucl Med, 2004. **45**(10): p. 1611-8.
68. Perin, E.C., et al., *Assessing myocardial viability and infarct transmurality with left ventricular electromechanical mapping in patients with stable coronary artery disease: validation by delayed-enhancement magnetic resonance imaging.* Circulation, 2002. **106**(8): p. 957-61.
69. Altehoefer, C., et al., *Significance of defect severity in technetium-99m-MIBI SPECT at rest to assess myocardial viability: comparison with fluorine-18-FDG PET.* J Nucl Med, 1994. **35**(4): p. 569-74.
70. Koch, K.C., et al., *Myocardial viability assessment by endocardial electroanatomic mapping: comparison with metabolic imaging and functional recovery after coronary revascularization.* J Am Coll Cardiol, 2001. **38**(1): p. 91-8.

71. Gepstein, L., G. Hayam, and S.A. Ben-Haim, *A novel method for nonfluoroscopic catheter-based electroanatomical mapping of the heart. In vitro and in vivo accuracy results.* Circulation, 1997. **95**(6): p. 1611-22.
72. Gepstein, L., et al., *Hemodynamic evaluation of the heart with a nonfluoroscopic electromechanical mapping technique.* Circulation, 1997. **96**(10): p. 3672-80.
73. Amado, L.C., et al., *Accurate and objective infarct sizing by contrast-enhanced magnetic resonance imaging in a canine myocardial infarction model.* J Am Coll Cardiol, 2004. **44**(12): p. 2383-9.
74. Koch, K.C., et al., *Prognostic value of endocardial electromechanical mapping in patients with left ventricular dysfunction undergoing percutaneous coronary intervention.* Am J Cardiol, 2004. **94**(9): p. 1129-33.
75. Kornowski, R., M.K. Hong, and M.B. Leon, *Comparison between left ventricular electromechanical mapping and radionuclide perfusion imaging for detection of myocardial viability.* Circulation, 1998. **98**(18): p. 1837-41.
76. van der Vleuten, P.A., et al., *Value and limitations of electromechanical endocardial mapping in the assessment of global and regional left ventricular function and transmural extent of infarction: a comparison with cardiovascular magnetic resonance.* EuroIntervention, 2010. **6**(5): p. 616-22.
77. Samady, H., et al., *Electromechanical mapping for detecting myocardial viability and ischemia in patients with severe ischemic cardiomyopathy.* Am J Cardiol, 2003. **91**(7): p. 807-11.
78. Botker, H.E., et al., *Electromechanical mapping for detection of myocardial viability in patients with ischemic cardiomyopathy.* Circulation, 2001. **103**(12): p. 1631-7.
79. Fallavollita, J.A., et al., *Spatial heterogeneity of endocardial voltage amplitude in viable, chronically dysfunctional myocardium.* Basic Res Cardiol, 2004. **99**(3): p. 212-22.
80. Keck, A., et al., *Electromechanical mapping for determination of myocardial contractility and viability. A comparison with echocardiography, myocardial single-photon emission computed tomography, and positron emission tomography.* J Am Coll Cardiol, 2002. **40**(6): p. 1067-74; discussion 1075-8.

81. Karsner, H.T. and J.E. Dwyer, *Studies in Infarction: IV. Experimental bland Infarction of the Myocardium, Myocardial Regeneration and Cicatrization.* J Med Res, 1916. **34**(1): p. 21-40 3.
82. Glick, G., *Importance of the carotid sinus baroreceptors in the regulation of myocardial performance.* J Clin Invest, 1971. **50**(5): p. 1116-23.
83. Gallagher, K.P., et al., *Significance of regional wall thickening abnormalities relative to transmural myocardial perfusion in anesthetized dogs.* Circulation, 1980. **62**(6): p. 1266-74.
84. Botvinick, E.H., et al., *Noninvasive quantitation of myocardial infarction with technetium 99m pyrophosphate.* Circulation, 1975. **52**(5): p. 909-15.
85. Weiss, E.S., et al., *Quantification of infarction in cross sections of canine myocardium in vivo with positron emission transaxial tomography and 11C-palmitate.* Circulation, 1977. **55**(1): p. 66-73.
86. Baks, T., et al., *Assessment of acute reperfused myocardial infarction with delayed enhancement 64-MDCT.* AJR Am J Roentgenol, 2007. **188**(2): p. W135-7.
87. Wyatt, H.L., et al., *Experimental evaluation of the extent of myocardial dyssynergy and infarct size by two-dimensional echocardiography.* Circulation, 1981. **63**(3): p. 607-14.
88. Sinusas, A.J., et al., *Quantification of area at risk during coronary occlusion and degree of myocardial salvage after reperfusion with technetium-99m methoxyisobutyl isonitrile.* Circulation, 1990. **82**(4): p. 1424-37.
89. Kim, R.J., et al., *Myocardial Gd-DTPA kinetics determine MRI contrast enhancement and reflect the extent and severity of myocardial injury after acute reperfused infarction.* Circulation, 1996. **94**(12): p. 3318-26.
90. Kim, R.J., et al., *The use of contrast-enhanced magnetic resonance imaging to identify reversible myocardial dysfunction.* N Engl J Med, 2000. **343**(20): p. 1445-53.
91. Fieno, D.S., et al., *Infarct resorption, compensatory hypertrophy, and differing patterns of ventricular remodeling following myocardial infarctions of varying size.* J Am Coll Cardiol, 2004. **43**(11): p. 2124-31.
92. Kim, R.J., et al., *Relationship of MRI delayed contrast enhancement to irreversible injury, infarct age, and contractile function.* Circulation, 1999. **100**(19): p. 1992-2002.

93. Lima, J.A., et al., *Regional heterogeneity of human myocardial infarcts demonstrated by contrast-enhanced MRI. Potential mechanisms.* Circulation, 1995. **92**(5): p. 1117-25.
94. de Roos, A., et al., *Reperfused and nonreperfused myocardial infarction: diagnostic potential of Gd-DTPA--enhanced MR imaging.* Radiology, 1989. **172**(3): p. 717-20.
95. Saeed, M., et al., *Discrimination of myocardial acute and chronic (scar) infarctions on delayed contrast enhanced magnetic resonance imaging with intravascular magnetic resonance contrast media.* J Am Coll Cardiol, 2006. **48**(10): p. 1961-8.
96. Hong, H., et al., *Remodeling of small intramyocardial coronary arteries distal to a severe epicardial coronary artery stenosis.* Arterioscler Thromb Vasc Biol, 2002. **22**(12): p. 2059-65.
97. Kirschner, R., et al., *Differentiation of acute and four-week old myocardial infarct with Gd(ABE-DTTA)-enhanced CMR.* J Cardiovasc Magn Reson, 2010. **12**: p. 22.
98. Kirschner, R., et al., *Acute infarct selective MRI contrast agent.* Int J Cardiovasc Imaging, 2011. **28**(2): p. 285-93.
99. Choi, S.I., et al., *Application of breath-hold T2-weighted, first-pass perfusion and gadolinium-enhanced T1-weighted MR imaging for assessment of myocardial viability in a pig model.* J Magn Reson Imaging, 2000. **11**(5): p. 476-80.
100. Garot, J., et al., *Magnetic resonance imaging of targeted catheter-based implantation of myogenic precursor cells into infarcted left ventricular myocardium.* J Am Coll Cardiol, 2003. **41**(10): p. 1841-6.
101. He, G., et al., *In vivo imaging of bone marrow mesenchymal stem cells transplanted into myocardium using magnetic resonance imaging: a novel method to trace the transplanted cells.* Int J Cardiol, 2007. **114**(1): p. 4-10.
102. Tallheden, T., et al., *In vivo MR imaging of magnetically labeled human embryonic stem cells.* Life Sci, 2006. **79**(10): p. 999-1006.
103. Simor, T., et al., *Percent infarct mapping for delayed contrast enhancement magnetic resonance imaging to quantify myocardial viability by Gd(DTPA).* J Magn Reson Imaging, 2010. **32**(4): p. 859-68.

104. Kirschner, R., et al., *Quantification of myocardial viability distribution with Gd(DTPA) bolus-enhanced, signal intensity-based percent infarct mapping.* Magn Reson Imaging, 2011. **29**(5): p. 650-8.
105. Wolf, T., et al., *Detailed endocardial mapping accurately predicts the transmural extent of myocardial infarction.* J Am Coll Cardiol, 2001. **37**(6): p. 1590-7.
106. Chazaud, B., et al., *Endoventricular porcine autologous myoblast transplantation can be successfully achieved with minor mechanical cell damage.* Cardiovasc Res, 2003. **58**(2): p. 444-50.
107. Kornowski, R., et al., *Electromagnetic guidance for catheter-based transendocardial injection: a platform for intramyocardial angiogenesis therapy. Results in normal and ischemic porcine models.* J Am Coll Cardiol, 2000. **35**(4): p. 1031-9.
108. Sylven, C., et al., *Catheter-based transendocardial myocardial gene transfer.* J Interv Cardiol, 2002. **15**(1): p. 7-13.
109. Charwat, S., et al., *Role of adult bone marrow stem cells in the repair of ischemic myocardium: current state of the art.* Exp Hematol, 2008. **36**(6): p. 672-80.
110. Gyongyosi, M., et al., *NOGA-guided analysis of regional myocardial perfusion abnormalities treated with intramyocardial injections of plasmid encoding vascular endothelial growth factor A-165 in patients with chronic myocardial ischemia: subanalysis of the EUROINJECT-ONE multicenter double-blind randomized study.* Circulation, 2005. **112**(9 Suppl): p. I157-65.
111. Cerqueira, M.D., et al., *Standardized myocardial segmentation and nomenclature for tomographic imaging of the heart: a statement for healthcare professionals from the Cardiac Imaging Committee of the Council on Clinical Cardiology of the American Heart Association.* Circulation, 2002. **105**(4): p. 539-42.
112. Fuchs, S., et al., *Comparison of endocardial electromechanical mapping with radionuclide perfusion imaging to assess myocardial viability and severity of myocardial ischemia in angina pectoris.* Am J Cardiol, 2001. **87**(7): p. 874-80.

9. List of publications

Publications related to the PhD thesis:

Articles published in international journals:

Lukács E, Magyari B, Tóth L, Petrási Zs, Repa I, Koller Á, Horváth I
Overview of large animal myocardial infarction models
Acta Physiol. 2012;99,4, 365-381
IF.: 0,821

Lukács E, Magyari B, Tóth L, Petrási Zs, Petneházy Ö, Simor T, Gyöngyösi M, Repa I, Koller Á, Rőth E, Horváth IG
Evaluation of experimental myocardial infarction models via electromechanical mapping and magnetic resonance imaging
Canadian Journal of Physiology and Pharmacology (accepted)
IF.: 1,953

Articles published in hungarian journals:

Lukács E, Kónyi A, Horváth I:
Az ivabradin alkalmazása miokardiális infarktuson átesett betegek körében – Irodalmi áttekintés az intervenciós kardiológus szemével
Card Hung, 40, 152-156 (2010)

Magyari B, **Lukács E**, Horváth I:
Az elektromechanikus térképezési rendszer (NOGA) szerepe a kardiológiában
Cardiologia Hungarica, 40:3, 216-220 (2010)

Abstracts:

Lukács E, Magyari B, Horváth I, Petrási Zs, Petneházy Ö, Seffer I, Simor T, Repa I: Embrionális őssejtek intramiokardiális implantációját követő bal kamra funkció és infarktus kiterjedés vizsgálata sertés infarktus modellen
MKT Kongresszus, Balatonfüred, 2010, presentation
Cardiologia Hungarica, 2010, 40, G:45

Lukács E, Magyari B, Horváth I, Petrási Zs, Petneházy Ö, Seffer I, Simor T, Repa I: A NOGA illetve MRI, mint diagnosztikus vizsgálatok összehasonlítása kísérletes szívinfarktusban sertés modellen
MKT Kongresszus, Balatonfüred, 2010, poster
Cardiologia Hungarica, 2010, 40, G:64

Edit Lukács, Balázs Magyari, Örs Petneházy, Zsolt Petrási, Levente Tóth, Imre Repa, Iván Horváth:
Characterisation of the Infarcted Myocardium via an Electroanatomical Mapping System in Different Porcine Models of Myocardial Infarction
Sixth International Conference on Cell Therapy for Cardiovascular Disease, 2011, poster

Lukács E, Magyari B, Tóth L., Petrási Zs, Petneházy Ö, Simor T, Repa I, Horváth I,: Különböző állatkísérletes modellen létrehozott miokardiális infarktus jellemzőinek vizsgálata elektromechanikus térképezési rendszer segítségével
MKT Kongresszus, Balatonfüred, 2011, presentation
Cardiologia Hungarica, 2011, 41, F:36

Edit Lukács, Balázs Magyari, Örs Petneházi, Zsolt Petrási, Levente Tóth, Imre Repa, Iván Horváth:
Comparison of two different myocardial infarction models in porcine utilizing electromechanical mapping system validated by cardiovascular magnetic resonance imaging
ESC congress, 2011, poster

Lukács E, Magyari B, Petneházy Ö, Petrási Zs, Tóth L, Simor T, Repa I, Rőth E, Horváth I

Investigation of two different myocardial infarction models in porcine from the aspect of myocardial viability via non-invasive and invasive methods

Conference & Advanced Research Workshop, Sudden Cardiac Death & Cardioprotection, Temesvár, 2012, poster

E. Lukács, B. Magyari, Ö. Petneházy, Zs. Petrási, L. Tóth, T. Simor, I. Repa, Á. Koller, IG Horváth:

Evaluation of experimental reperfused and nonreperfused myocardial infarction models from the aspect of myocardial viability via magnetic resonance imaging

8th International Conference on Cell Therapy for Cardiovascular Disease, 2013, poster

Publications not related to the PhD thesis:

Lukács E., Magyari B., Horváth I.:

Unusual thrombectomy in acute myocardial infarction

Euro PCR, Párizs, 2010, presentation

Lukács E, Horváth I:

A frekvenciakontroll jelentősége a centrális vérnyomás és a szívfrekvencia variabilitás tükrében

Cardiologia Hungarica, 42, 100-105 (2012)

Acknowledgements:

First of all, I would like to thank my mentor and supervisor Iván Horváth for his guidance in research and generous support. I would like to express my gratitude to Professor Erzsébet Rőth and to Professor Ákos Koller for their scientific support and mentorship. I would like to express my special thanks to Balázs Magyari, for assisting my work and for his generous support. I am grateful to Professor Tamás Simor and Levente Tóth, to give me valuable scientific information and useful advises. I would like to express my gratitude to Professor Sándor Szabados for his generous support during my studies. The studies were carried out at the Institute of Diagnostic and Therapeutic Radiation, at the University of Kaposvár. I would like to express my gratitude to Professor Imre Repa, for raising our research ideas into reality, and to Zsolt Petrási, Örs Petneházy, Gergő Szabó and István Takács, for their contribution to our experiments. I am thankful to all the nurses and technicians for their kind help especially to Anita Háberkorn, Brigitta Witzl and Brigitta Németh.

This work was supported by grants from the Hungarian Scientific Research Fund (OTKA K-69118 and K-71591) and by the Foundation for Improvement of Interventional Cardiology (Nr. 1478).

Finally I express my thanks to my family and friends for their encouraging support throughout my studies and work.